Ref.TH.1661-CERN

$\pi\pi$ PHASE SHIFT ANALYSIS*

P. Estabrooks+ and A.D. Martin"
Theory Division, CERN, Geneva

G. Grayer⊕, B. Hyams, C. Jones and P. Weilhammer
Nuclear Physics Division, CERN, Geneva

W. Blum, H. Dietl, W. Koch, E. Lorenz, G. Lütjens,
W. Männer, J. Meissburger and U. Stierlin
Max-Planck-Institut für Physik und Astrophysik,
Munich

ABSTRACT

We perform an energy independent $\pi\pi$ phase shift analysis in the energy range $440 < M_{\pi\pi} < 1400$ MeV using high statistics $\pi^- p \to \pi^- \pi^+ n$ data at 17.2 GeV/c. The method is based on an amplitude analysis of the production process and the extrapolation of the dominant π exchange amplitudes to the π exchange pole. We consider the phase shift ambiguities and study ways of selecting the physical solution. We determine the parameters of the ρ and f resonances. We find an $I = 0$ S wave resonance under the f and we comment on the properties of the S^* resonance near the $K\bar{K}$ threshold.

---

* Invited talk by A.D. Martin at the International Conference on $\pi\pi$ Scattering and Associated Topics, Tallahassee, Fl. March 28-30, 1973.

+ Supported by the National Research Council of Canada.

" On leave of absence from the University of Durham, England.

⊕ Now at the Max-Planck-Institut, Munich.

Ref.TH.1661-CERN

7 May 1973

1. INTRODUCTION

It was originally proposed by Goebel[1] and by Chew and Low[2] that the $\pi N \to \pi\pi N$ cross-section suitably extrapolated from the physical region to the π exchange pole $(t = \mu^2)$ would provide a valuable means of determining the $\pi\pi$ differential cross-section. Many attempts to extract $\pi\pi$ phases have been based on Chew-Low extrapolations, until now agreement has been reached on the general picture of the phases in the ρ region[3]. However, with the recent increase in experimental statistics of the $\pi^- p \to \pi^- \pi^+ n$ data we are confronted with the problem of finding the best way to account for the other exchange mechanisms which

are seen to occur in addition to π exchange. The method we propose is to use the observed moments of the $\pi^-\pi^+$ angular distribution to perform an amplitude analysis of the production process. In this way we can isolate the dominant π exchange pole. That we are able to perform such an amplitude analysis without knowledge of the nucleon polarization observables is a fortunate circumstance of the nature of the exchanges (see Section 3).

We use this method to extract $\pi\pi$ phase shifts from the high statistics $\pi^-p\to\pi^-\pi^+n$ data at 17.2 GeV/c[4]. We discuss separately the $\pi\pi$ phase shift analysis below and above the $K\bar{K}$ threshold. The former is described in Sections 4-6 and the latter in Section 7. In Section 8 we comment on the behaviour of the $I=0$ $\pi\pi$ S wave near the $K\bar{K}$ threshold.

2. PION EXCHANGE

Suppose that the reaction $\pi^-p\to(\pi^-\pi^+)n$ were mediated entirely by π exchange. Then the differential cross-section is

$$\frac{d^3\sigma}{dt\,dM_{\pi\pi}\,d\Omega} = \frac{2}{4\pi m^2 p_L^2}\left(\frac{g^2}{4\pi}\right)\frac{-t}{(t-\mu^2)^2}\left|F(t)\right|^2 q\,M_{\pi\pi}^2\,\frac{d\sigma_{\pi\pi}}{d\Omega} \qquad (1)$$

where m is the nucleon mass, p_L is the incident π^- laboratory momentum, t is the momentum transfer at the nucleon vertex, $F(t)$ a form factor satisfying $F(\mu^2)=1$, and the πNN coupling $g^2/4\pi = 14.4$. q, $M_{\pi\pi}$ and $d\sigma_{\pi\pi}/d\Omega$ are the $\pi^-\pi^+$ momentum, mass and differential cross-section in the $\pi^-\pi^+$ c.m. frame.

The experimental observables are the moments $\langle Y_M^J\rangle$ of the $\pi^-\pi^+$ angular distribution as a function of t and $M_{\pi\pi}$

$$\frac{d^3\sigma}{dt\,dM_{\pi\pi}\,d\Omega} = N\sum_J\sum_{M=-J}^{J}\langle Y_M^J\rangle\,\mathrm{Re}\,Y_M^J(\theta,\phi) \qquad (2)$$

where N is the number of events in the element $dt\,dM_{\pi\pi}$ and where we have chosen the y axis normal to the $\pi^-p\to(\pi\pi)n$ reaction plane. We use $\langle Y_M^J\rangle$ to abbreviate $\mathrm{Re}\langle Y_M^J\rangle$.

π exchange produces only (t channel) helicity zero $\pi^-\pi^+$ systems, and in this simplified situation only the $M=0$ moments, $\langle Y_0^J\rangle$, would be non-zero. We may express these moments in terms of the $(\pi^-p\to\pi^-\pi^+n)$ amplitudes for the production of S, P,... wave helicity zero $\pi^-\pi^+$ states

$$\sqrt{4\pi}\, N \langle Y_0^0 \rangle = |S_0|^2 + |P_0|^2 + \ldots.$$
$$\sqrt{4\pi}\, N \langle Y_0^1 \rangle = 2\,\mathrm{Re}\,(S_0 P_0^*) + \ldots. \qquad (3)$$
$$\sqrt{4\pi}\, N \langle Y_0^2 \rangle = \frac{2}{\sqrt{5}} |P_0|^2 + \ldots$$

where the omitted terms involve D_0, F_0,... Up to a normalization constant these amplitudes are given by

$$L_0 = \frac{\sqrt{-t}}{t-\mu^2} F_L(t) \frac{M_{\pi\pi}}{\sqrt{q}} \sqrt{2L+1}\, f_L \qquad (4)$$

where f_L are the $\pi^-\pi^+$ partial wave amplitudes at c.m. energy $M_{\pi\pi}$

$$f_L = f_L^{I=1} \qquad \text{for } L \text{ odd}$$
$$f_L = \tfrac{2}{3} f_L^{I=0} + \tfrac{1}{3} f_L^{I=2} \qquad \text{for } L \text{ even.} \qquad (5)$$

The f_L are defined so that in the $\pi\pi$ elastic region

$$f_L^I = \sin\delta_L^I \; e^{i\delta_L^I} \qquad (6)$$

Thus $\pi\pi$ phases can be obtained by extrapolating the production amplitudes, or rather $(t-\mu^2)L_0/\sqrt{-t}$, from the physical region $(t<0)$ to $t=\mu^2$.

In Fig. 1 we show the mass spectrum up to $M_{\pi\pi} = 2$ GeV of the unnormalized t channel moments integrated over the interval $0 < -t < 0.15$ GeV^2 obtained in $\pi^-p \to \pi^-\pi^+n$ at 17.2 GeV/c . From these moments we see :

a) the presence of the $\rho(770)$, $f(1260)$, $g(1700)$ mesons with spins 1, 2, 3 respectively ; to establish[6,4] spin 3 for the g meson requires the additional knowledge that the $J = 7$ and higher moments are small near 1700 MeV ;

b) from $\langle Y_0^1 \rangle$ the presence of a large S wave under the ρ meson ;

c) from $\langle Y_0^2 \rangle$ the presence of a large S wave under the f meson[7] ;

d) sharp structure near $M_{\pi\pi} = 1$ and 1.45 GeV which Odorico[8] associates with the double pole killing zeros propagating linearly into the $\pi^-\pi^+$ physical region from the forward

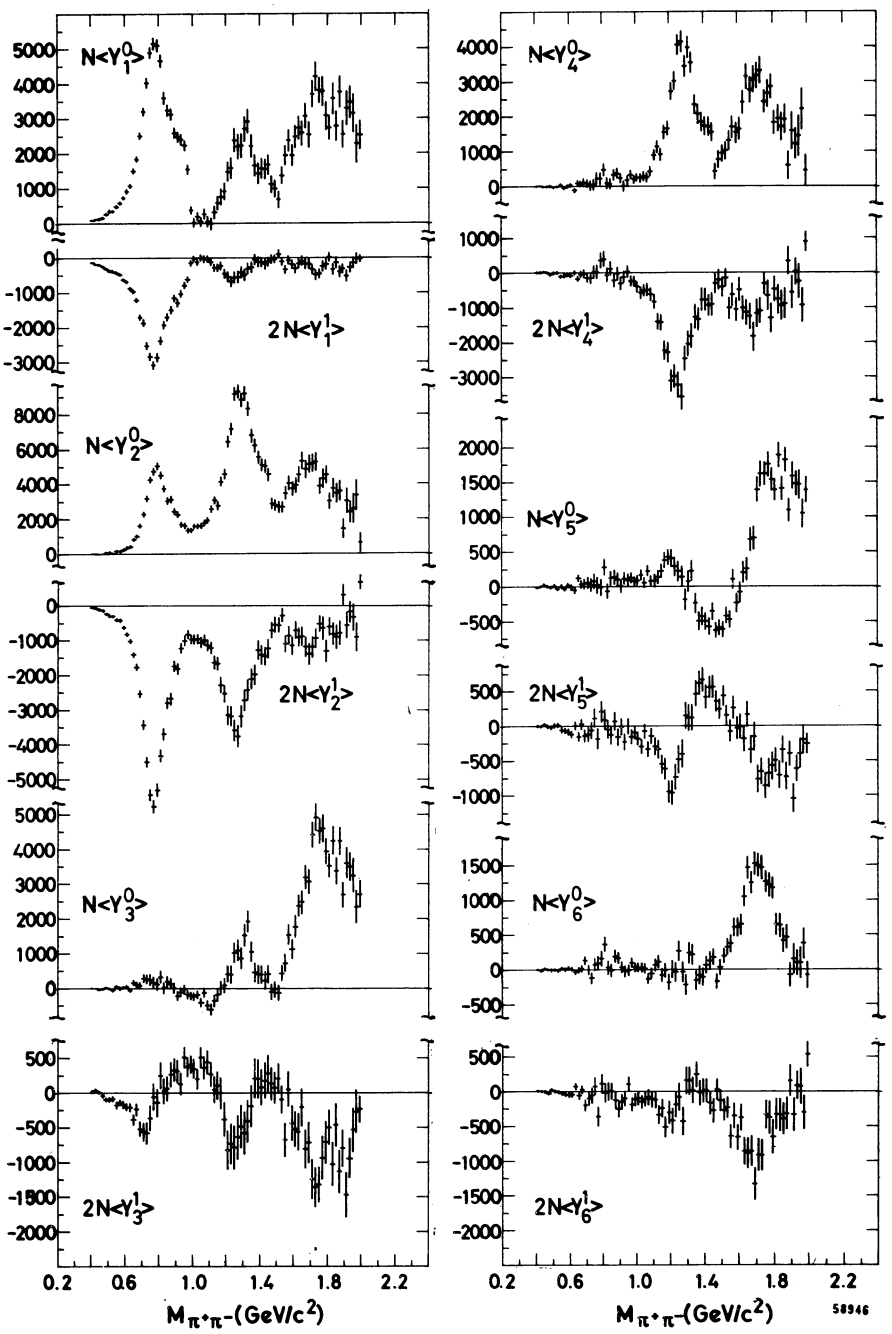

Figure 1 The corrected unnormalized t channel moments, $N < Y_J^M >$, as a function of $\pi^+\pi^-$ mass for the interval $0 < -t < 0.15$ GeV^2, taken from Ref. 4. A factor of 2 should be included in the $M \neq 0$ moments shown in Ref. 5.

direction ; the effect at 1 GeV is complicated by the opening of the $K\bar{K}$ channel with the cross-section at its S wave unitarity limit, suggesting the nearby presence of the S^* meson[9] ;

e) from $< Y_1^J >$ moments the non-negligible presence of helicity one $\pi^-\pi^+$ production.

This last observation indicates that there are other exchange mechanisms in addition to π exchange, such as A_2 exchange or absorptive corrections. Thus a $\pi\pi$ phase shift analysis based on a straightforward extrapolation of the $< Y_0^J >$ moments can be very misleading[10,11]. Additional terms occur on the right-hand sides of Eqs. (3) involving amplitudes describing non-zero helicity $\pi\pi$ production. To allow for these exchanges we perform a production amplitude analysis of all the observed moments as a function of t and $M_{\pi\pi}$.

3. AMPLITUDES AND EXCHANGE MECHANISMS FOR $\pi^- p \to \pi^- \pi^+ n$

To describe the reaction $\pi^- p \to \pi^- \pi^+ n$ we use the variables shown in Fig. 2. The production of a $\pi^-\pi^+$ system of spin L is described by helicity amplitudes $H^{L,\lambda}(s,t,M^2_{\pi\pi})$ with $\pi\pi$ helicity $\lambda = 0, \pm 1, \ldots, \pm L$. For the moment we omit the nucleon helicity labels. This simplifies the discussion and will be corrected for later.

It is convenient to introduce the combinations of helicity amplitudes

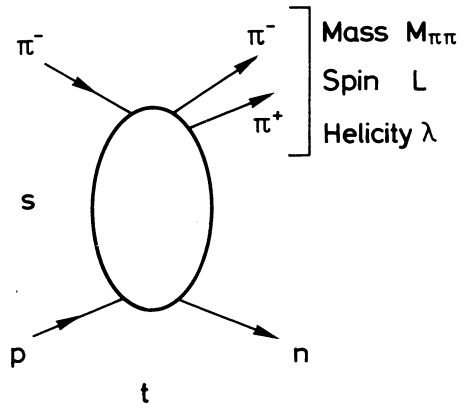

Figure 2 Variables for the process $\pi^- p \to \pi^- \pi^+ n$.

$$L_{\lambda\pm} = \frac{1}{\sqrt{2}} \left(H^{L,\lambda} \mp (-1)^\lambda H^{L,-\lambda} \right). \qquad (7a)$$

At high energies (that is, to order 1/s) the amplitudes $L_{\lambda+}$ and $L_{\lambda-}$ describe the production of a $\pi\pi$ system of spin L, helicity λ by natural and unnatural parity exchange, respectively. We see that $L_{\lambda+} = 0$ for $\lambda = 0$ $\pi\pi$ production, that is, a zero helicity $\pi\pi$ system cannot be produced at high energies by natural parity exchange. In this case we have only an unnatural parity exchange amplitude, which we define as

$$L_0 \equiv H^{L,0} \qquad (7b)$$

The observables $< Y_M^J >$ may be expressed in terms of the amplitudes $(S_0, P_0, P_{1\pm}, D_0, D_{1\pm}, D_{2\pm}, \ldots)$ of Eqs. (7). Each moment is a sum over bilinear terms of the form $\mathrm{Re}(L'_\lambda, L^*_\lambda)$. A given moment $< Y_M^J >$ will only contain terms with $L' + L \geq J$ and $|\lambda' - \lambda| = M$. Furthermore $L' + L$ must be even (odd) if J is even (odd). These restrictions are embodied in the Clebsch-Gordan coefficients $< LL'\lambda - \lambda' | JM >$ and $< LL'00 | J0 >$ which occur when the density matrix is expressed in terms of the moments[12]. Moreover, the moments contain no interference terms between L_{λ_+} and L_{λ_-} amplitudes.

For example, in a region of $M_{\pi\pi}$ where only S and P wave $\pi\pi$ production is appreciable, the observables can be expressed in terms of the production amplitudes $S_0, P_0, P_{1\pm}$ as follows

$$\sqrt{4\pi}\, N \langle Y_0^0 \rangle = |S|^2 + |P_0|^2 + |P_+|^2 + |P_-|^2$$

$$\sqrt{4\pi}\, N \langle Y_0^1 \rangle = 2\,\mathrm{Re}\,(S P_0^*)$$

$$\sqrt{4\pi}\, N \langle Y_1^1 \rangle = \sqrt{2}\,\mathrm{Re}\,(S P_-^*)$$

$$\sqrt{4\pi}\, N \langle Y_0^2 \rangle = \frac{1}{\sqrt{5}} \left(2|P_0|^2 - |P_+|^2 - |P_-|^2 \right) \qquad (8)$$

$$\sqrt{4\pi}\, N \langle Y_1^2 \rangle = \sqrt{\frac{6}{5}}\,\mathrm{Re}\,(P_0 P_-^*)$$

$$\sqrt{4\pi}\, N \langle Y_2^2 \rangle = -\sqrt{\frac{3}{10}} \left(|P_+|^2 - |P_-|^2 \right)$$

So far we have simplified the discussion by disregarding the nucleon helicities. Each amplitude is really two independent amplitudes, a nucleon helicity flip and a non-flip amplitude, $H^{L,\lambda}_{+-}$ and $H^{L,\lambda}_{++}$ respectively. The combinations of Eqs. (7) are to be formed for both the nucleon flip and non-flip amplitudes. For an experiment involving unpolarized nucleons, Eqs. (8) are correct provided it is understood that the nucleon helicities are summed over as follows

$$|L|^2 \equiv |L_{++}|^2 + |L_{+-}|^2$$

$$\mathrm{Re}\,(L' L^*) \equiv \mathrm{Re}\,(L'_{++} L^*_{++} + L'_{+-} L^*_{+-}) \qquad (9)$$

Here we have omitted the $\pi\pi$ helicity label.

The absence of nucleon polarization data prevents a model independent determination of the amplitudes for $\pi N \to (\pi\pi)N$. However, the unnatural parity exchanges have the simplifying property* that π exchange contributes only to nucleon flip amplitudes, whereas the amplitudes with the quantum numbers of A_1 exchange have nucleon non-flip (cf. Table I). We shall call the latter A_1 exchange contributions regardless of whether they arise from A_1 exchange, absorption, etc., with the exception of the order $1/s$ π exchange contribution in the s channel which we include explicitly. A study of the eigenvalues of the density matrix within the positivity domain[13] indicates that the A_1 contributions are small. Here we shall neglect these contributions. This should be a good approximation, particularly as the neglected quantities only enter quadratically in the expressions for the observables $< Y_M^J >$, that is, there are no π-A_1 interference terms.

The most direct check of this assumption will be nucleon polarization measurements for $\pi N \to \pi\pi N$; the polarization associated with unnatural parity exchange is due to π-A_1 interference. Also we can check the small t dependence of the observable $(3\rho_{00}^P + \rho_{00}^S)d\sigma/dt$ in a $\pi\pi$ mass region where S and P waves are dominant. The π exchange contribution vanishes like t in contrast to the non-flip A_1 contribution. In practice this test[14] is difficult, requiring very high statistics and depending mainly on the extreme forward data points.

With the assumption of negligible A_1 exchange contributions it follows, for example, that the relative phases

$$\varphi = \arg(P_-) - \arg(P_0)$$
$$\Delta = \arg(S_0) - \arg(P_0) \qquad (10)$$

determine the phase between S_0 and P_-. Thus in a region of $M_{\pi\pi}$ where only S and P wave $\pi^-\pi^+$ states are important we can use the six observable moments, Eqs. (8), to determine[15] $|P_+|$, $|P_0|$, $|P_-|$, $|S|$, φ and Δ as functions of $M_{\pi\pi}$ and t. In Section 4 we discuss the uniqueness of the solution and also how we include the small D wave contribution.

---

* This is exactly true for the π pole in the t channel; in the s channel we have order $1/s$ π exchange contributions to the nucleon non-flip amplitudes.

s ch. hel. amp. $H^{L,\lambda}_{\lambda_n,\lambda_p}$	n, x	ang. mom. $(\sqrt{-t'})^n$	Regge pole exchange	
			nat. p. ($L_{\lambda+}$) / unnat. p. ($L_{\lambda-}$)	$(\sqrt{-t'})^{n+x}$
$H^{L,0}_{+-}$	1 0	$\sqrt{-t'}$	π	$\sqrt{-t'}$
$H^{L,0}_{++}$	0 0	const	A_1	const
$H^{L,1}_{+-}$	0 2	const	$A_2 + \pi$	$-t'$
$H^{L,-1}_{+-}$	2 0	t'	$A_2 - \pi$	$-t'$
$H^{L,1}_{++}$	1 0	$\sqrt{-t'}$	$A_2 + A_1$	$\sqrt{-t'}$
$H^{L,-1}_{++}$	1 0	$\sqrt{-t'}$	$A_2 - A_1$	$\sqrt{-t'}$
$H^{L,2}_{+-}$	1 2	$\sqrt{-t'}$	$A_2 + \pi$	$(\sqrt{-t'})^3$
$H^{L,-2}_{+-}$	3 0	$(\sqrt{-t'})^3$	$-A_2 + \pi$	$(\sqrt{-t'})^3$
⋮				

TABLE I : Regge exchange contributions to the s channel helicity amplitudes for $\pi^-p \to (\pi^-\pi^+)n$ and their behaviour in the forward direction, $t' \equiv t - t_{min} = 0$. λ is the helicity of the $\pi^-\pi^+$ system. The amplitudes $L_{\lambda+}$ and $L_{\lambda-}$ are defined in Eqs. (7). To leading order in s, only the exchanges listed contribute to $L_{\lambda+}$ and $L_{\lambda-}$.

Choice of frame and absorptive corrections :

In order to extract $\pi\pi$ phase shifts we must isolate the $\pi N \to (\pi\pi)N$ amplitudes which are dominated by π pole exchange and suitably extrapolate them from the physical region to $t = \mu^2$. Clearly S_0, P_0, D_0,... are the desired amplitudes. Now the amplitude analysis can be done equally well using either the s or t channel moments of the $\pi^+\pi^-$ angular distribution. However, we argue that it is appropriate to extrapolate s channel amplitudes. The reason is that we believe the absorptive corrections to the exchange pole contributions are simpler in the s channel[16]. At present we do not have a reliable prescription for determining these corrections. The indications are that they interfere destructively with the pole contributions and that, to a good approximation, they conserve s channel helicities. Moreover they are expected to be largest in $x \neq 0$ s channel amplitudes, and, for $x = 0$ amplitudes, to decrease with increasing net helicity flip n (the n,x notation is that of Ref. 16). For an s channel helicity amplitude the net helicity flip, $n = |\lambda + \lambda_p - \lambda_n|$, specifies the forward behaviour arising from angular momentum conservation, and $n + x = |\lambda| + |\lambda_p - \lambda_n|$, specifies the behaviour for definite parity (Regge pole) exchange. This behaviour, together with the values of n and x, is listed in Table I.

Consider the $x = 2$ $H^{L,1}_{+-}$ s channel helicity amplitude. The pole contributions, which are required to vanish as t', are expected to be modified by destructive interference with a non-vanishing (absorptive) background. The cross-over zeros in the s channel $\langle Y^0_1 \rangle$ moments near $-t = \mu^2$ are experimental support for this picture. This absorptive correction to the s channel P_{1-}, D_{1-},... amplitudes will, when crossed, affect the t channel P_0, D_0,... helicity amplitudes. Of course, the s channel S_0, P_0,... amplitudes may themselves have absorptive corrections, but as these are helicity flip amplitudes these modifications should be relatively small. In either channel the absorptive modifications to S_0, P_0, D_0,... do not in principle cause a problem since they should disappear on appropriate extrapolation to the π exchange pole. However, to determine $\pi\pi$ phases it is desirable to extrapolate what are believed to be the "purest" π exchange amplitudes and for this reason we shall use the s channel S_0, P_0, D_0,... amplitudes.

One slight complication of this choice is that the π pole contribution, which in the t channel contributes only to S_0, P_0,..., is distributed among all the $L_{\lambda-}$ s channel amplitudes. For example, for P wave $\pi^+\pi^-$ production we have, to leading order in s,

$$(P_0)_{+-} \equiv H^{1,0}_{+-} = -\frac{g_{\pi}}{\sqrt{q}} \frac{t + M^2_{\pi\pi} - \mu^2}{J} \frac{\sqrt{-t'}}{t - \mu^2} \qquad (11)$$

$$(P_-)_{+-} = \frac{g_\pi}{\sqrt{q}} \frac{2M_{\pi\pi}}{J} \frac{t'}{t-\mu^2}$$

$$(P_0)_{++} \equiv H^{1,0}_{++} = r\, H^{1,0}_{+-} \qquad \text{with } r = \sqrt{\frac{t_{min}}{t'}} \qquad (11)$$

where $J^2 \equiv \left[t - (M_{\pi\pi\pi} - \mu)^2\right]\left[t - (M_{\pi\pi\pi} + \mu)^2\right] \simeq M^2_{\pi\pi\pi}$.

The last amplitude is only relevant at very small t. To include its contribution we multiply each product of $\lambda = 0$ amplitudes (e.g., $|P_0|^2$, $\mathrm{Re}(S_0 P_0^*)$) occurring in the expressions for the observable moments, Eqs. (8), by $1 + r^2$ before solving for the amplitudes[15]. Thus from now on by S_0, P_0,... we mean only the helicity flip amplitudes $H^{L,0}_{+-}$.

4. PRODUCTION AMPLITUDE ANALYSIS FOR $M_{\pi\pi\pi}$ BELOW 1 GeV

We have seen that the neglect of A_1 exchange amplitudes permits the determination of the magnitudes and relative phases of the amplitudes (S, P_0, P_-) and the magnitude of P_+ directly from the data. Instead of using the relative phases φ and Δ of Eq. (10) it is convenient to project S and P_- into components parallel and perpendicular to P_0 on the Argand plot as illustrated in Fig. 3. In terms of these amplitude components the moments of the $\pi^-\pi^+$ angular distribution become

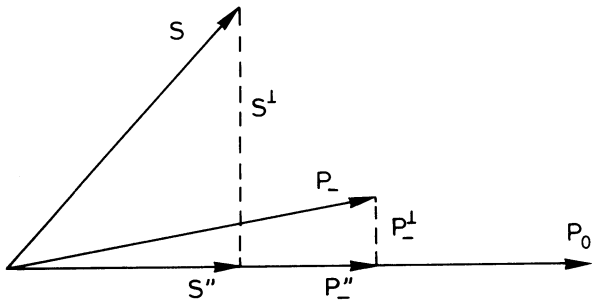

Figure 3 Vectors representing the unnatural parity exchange amplitudes. The components $S^{\parallel}$, $P^{\parallel}_-$ and $P^{\perp}_-$ are well determined by the data, whereas essentially only the product of the perpendicular components, $S^{\perp}\, P^{\perp}_-$, is measured.

$$\sqrt{4\pi}\, N \langle Y_0^0 \rangle = |S''|^2 + |S^\perp|^2 + |P_0|^2 + |P_+|^2 + |P_-''|^2 + |P_-^\perp|^2$$

$$\sqrt{4\pi}\, N \langle Y_0^1 \rangle = 2 S'' |P_0|$$

$$\sqrt{4\pi}\, N \langle Y_1^1 \rangle = \sqrt{2}\,(S'' P_-'' + S^\perp P_-^\perp)$$

$$\sqrt{4\pi}\, N \langle Y_0^2 \rangle = \frac{1}{\sqrt{5}}\left(2|P_0|^2 - |P_+|^2 - |P_-''|^2 - |P_-^\perp|^2\right)$$

$$\sqrt{4\pi}\, N \langle Y_1^2 \rangle = \sqrt{\frac{6}{5}}\, P_-'' |P_0|$$

$$\sqrt{4\pi}\, N \langle Y_2^2 \rangle = -\sqrt{\frac{3}{10}}\left(|P_+|^2 - |P_-''|^2 - |P_-^\perp|^2\right)$$

(12)

Eliminating all amplitude components in favour of $|P_0|$ we obtain a cubic equation for $|P_0|^2$. From the observed moments it turns out that one solution is unphysical, $|P_0|^2 < 0$, and that the remaining two solutions are both physical with similar values of $|P_0|^2$.

We are considering a region of $M_{\pi\pi}$ where D waves are relatively small. Although in Eqs. (12) we have omitted the terms depending on the D wave amplitudes we do, in fact, allow for these small contributions. In the first place we solve analytically for the two solutions using $\langle Y_0^1 \rangle - \sqrt{28/27}\langle Y_0^3 \rangle$ instead of $\langle Y_0^1 \rangle$ since, unlike $\langle Y_0^1 \rangle$, this combination does not contain the dominant D wave interference term $\mathrm{Re}(P_0 D_0^*)$. Moreover using the $\langle Y_0^3 \rangle$ moment we estimate D_0, $D_{1\pm}$ as described in Section 5.b. We allow for these small D wave contributions in the S and P wave amplitude analysis by iteration starting from the two exact solutions.

As an example we show in Fig. 4 the two solutions found at the different t values from the s channel moments in the mass bin $700 < M_{\pi\pi} < 720$ MeV. The amplitudes S and P_0 have similar t behaviour and so we show $\gamma_S^\perp = S^\parallel/|P_0|$ and $\gamma_S^\perp = S^\perp/|P_0^\perp|$. By inspection of Eqs. (12) we notice that the component $S^\perp$ is less constrained than $S^\parallel$ and this is reflected in the resulting errors. Similarly the component $P_-^\parallel$ is better determined than $P_-^\perp$. Moreover, the data do not determine the absolute signs of $S^\perp$ and $P_-^\perp$, but only their relative sign. In the ambiguous cases we have chosen $P_-^\perp$ to be positive in Fig. 4.

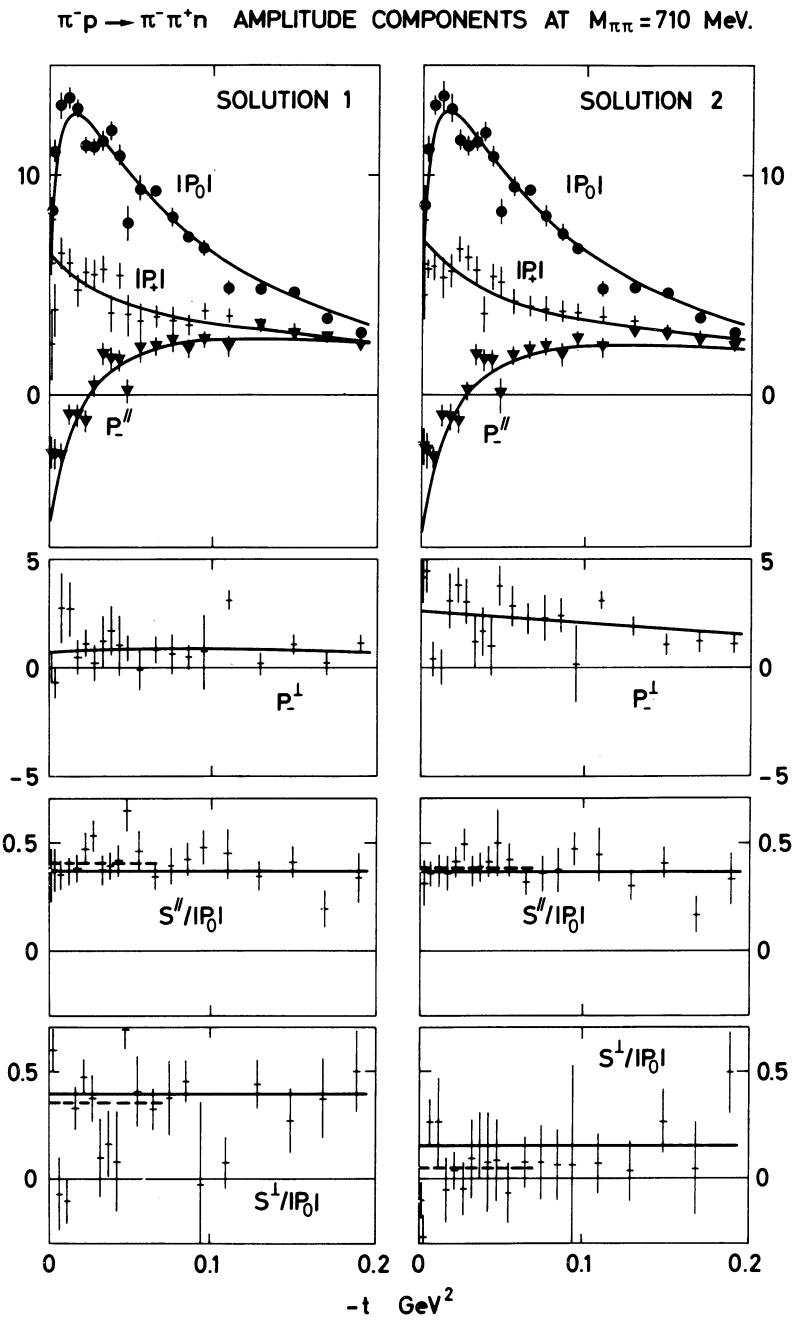

Figure 4 The two solutions for the s channel amplitude components calculated from the data in the mass bin $700 < M_{\pi\pi} < 720$ MeV. The points are the solutions obtained at the different t values and the dashed lines represent the resulting average values of S/P_0. The continuous lines are obtained from the parametric fit to the data that is described in Section 5.

We may compare the structure of these amplitude components with the behaviour anticipated from the contributions of π exchange to P_0 and P_-, and A_2 exchange to P_+ (cf. Section 3). Up to slope factors of the form $\exp[b(t-\mu^2)]$, the P wave amplitudes are expected to have the following t structure

$$P_0 = -g_\pi \delta_\pi M_{\pi\pi} \frac{\sqrt{-t'}}{t-\mu^2}$$

$$P_- = g_\pi \left[\delta_\pi \frac{2t'}{t-\mu^2} - C(t)\right] \qquad (13)$$

$$|P_+|^2 = \left|-t' g_A^F \delta_A - g_\pi C(t)\right|^2 - t' \left|g_A^{NF} \delta_A\right|^2$$

to leading order in s, where δ_i are signature factors $\frac{1}{2}+\frac{1}{2}\exp(-i\pi\alpha_i)$ with $\alpha_\pi \approx t-\mu^2$ and $\alpha_A \approx 0.5 + t$, and g_A^F and g_A^{NF} are the A_2 exchange couplings to nucleon helicity flip and non-flip respectively. Studies[17] of ρ and A_2 exchange in spin 0 - spin $\frac{1}{2}$ processes indicate that there $g_A^F/g_A^{NF} \approx 4$. The additional contribution $g_\pi C(t)$, which is non-vanishing at $t' = 0$, can be regarded as the absorptive correction to π and A_2 exchange in the (evasive) s channel H^1_{+-} amplitude. At $t' = 0$ we have $P_+ = P_-$. The Williams' model[18] is a special case of Eqs. (13), namely that with $g_A^{F,NF} = 0$, $\delta_\pi = 1$ and $C = 1$.

For the amplitudes obtained from the data in the ρ mass band, $730 < M_{\pi\pi} < 810$ MeV, such a breakdown has been discussed in Ref. 15 (see also Refs. 19, 20). The actual interpretation of the various contributions to $P_\pm$ is not important as far as the extraction of $\pi\pi$ phases is concerned. However, $P_\pm$ give sizeable contributions to all the moments and it is crucial to allow for their presence in the Chew-Low extrapolation.

The two allowed solutions for the amplitude components are distinguished mainly by their differing values of $S^\perp$ and this leads to an ambiguity in the determination of the $\pi\pi$ S wave phase.

Connection with $\pi\pi$ phases :

For each $M_{\pi\pi}$ bin the dominant π exchange amplitudes, S and P_0, are the appropriate quantities to extrapolate in t to $t = \mu^2$ to determine $\pi\pi$ phase shifts. We discuss first the P wave and then the S wave extrapolation.

To extrapolate $|P_0|$ to the π exchange pole we fit the calculated amplitudes for $-t < 0.2$ to the form [cf. Eq. (4)]

$$P_o = A \frac{\sqrt{-t'}}{\mu^2 - t} \; e^{b(t-\mu^2)} \sqrt{3} \, f_P , \qquad (14)$$

where for $M_{\pi\pi}$ in the $\pi^-\pi^+$ elastic region $f_P = \sin\delta_P \, e^{i\delta_P}$. In other words, from $|P_o|$ we determine $A|f_P|$ and thus, knowing the normalization A, we obtain δ_P, the P wave $\pi\pi$ phase shift. The normalization factor A has an $M_{\pi\pi}$ dependence

$$A^2 = \mathcal{N} \frac{M_{\pi\pi}^2}{q} \left[\frac{M_{\pi\pi}^2}{M_{\pi\pi}^2 - 4\mu^2} \right] , \qquad (15)$$

where $M_{\pi\pi}^2/q$ arises from the Chew-Low formula and the factor in brackets is due to crossing P_o from the t to the s channel at $t = \mu^2$. It remains to fix the over-all normalization constant, $\mathcal{N}$, of the $\pi^-p \to \pi^-\pi^+n$ cross-section $d\sigma/dM_{\pi\pi}$. To do this we extrapolate $|P_o|$ for each $M_{\pi\pi}$ bin in the region of the ρ resonance, and adjust the constant $\mathcal{N}$ until the resulting δ_P goes smoothly through the resonance. Knowing the constant $\mathcal{N}$, and therefore A, we can calculate δ_P as a function of $M_{\pi\pi}$ in the $\pi^-\pi^+$ elastic region.

Consider now the extrapolation of the S wave amplitudes. To a good approximation the values of S/P_o are constant in t. Therefore, to obtain the value at $t = \mu^2$, we simply fit the values for $-t < 0.2$ to a constant

$$\frac{S}{P_o} = \frac{\frac{2}{3} f_S^0 + \frac{1}{3} f_S^2}{\sqrt{3} \, f_P} \qquad (16)$$

At the sample energy, $M_{\pi\pi} = 710$ MeV, the resulting extrapolations for $S^{\parallel}/P_o$ and $S^{\perp}/P_o$ are indicated by dashed lines on Fig. 4.

It is illuminating to view the results in terms of the unitarity circles for the $\pi\pi$ partial wave amplitudes, f_L^I. We cannot determine both the $I = 0$ and $I = 2$ S wave $\pi\pi$ phase shifts and so we input f_S^2 using the values obtained in analyses [3,21] of $\pi^+p \to \pi^+\pi^+n$ data. The values we use for δ_S^2 are listed in Table II. The situation at 710 MeV is shown in Fig. 5. The larger unitarity circle corresponds to the P wave which we assume to be elastic. Then, as described above, $|P_o|$ determines δ_P. The P wave results for the two solutions are almost identical and are shown by a single line on Fig. 5. Also we show the unitarity circle for the $I = 0$ S wave, scaled down by the factor $2/3\sqrt{3}$ arising from $\sqrt{2L+1}$ and isospin.

$M_{\pi\pi}$	Solution 1				Solution 2				Input
(MeV)	δ^o_S	δ_P	δ^o_D	χ^2	δ^o_S	δ_P	δ^o_D	χ^2	δ^2_S
450	39.1 ± 2.7	4.8 ± 0.9	0.4	101	21.0 ± 3.4	7.6 ± 0.5	0.4	96	- 5.2
470	43.1 ± 1.8	6.2 ± 0.6	0.6	104	16.7 ± 2.4	9.9 ± 0.4	0.6	96	- 6.0
490	48.5 ± 2.0	7.9 ± 0.4	0.8	117	20.8 ± 2.6	11.5 ± 0.5	0.8	118	- 6.6
510	51.8 ± 2.2	9.3 ± 0.5	1.1	136	25.2 ± 2.7	12.2 ± 0.5	1.1	140	- 7.2
530	52.0 ± 2.2	10.0 ± 0.6	1.5	149	26.6 ± 3.3	13.1 ± 0.5	1.5	157	- 7.8
550	55.9 ± 2.3	11.5 ± 0.5	1.9	94	27.4 ± 3.5	14.6 ± 0.5	1.9	109	- 8.5
570	59.1 ± 2.7	12.5 ± 0.5	2.4	141	28.0 ± 3.6	15.3 ± 0.5	2.4	153	- 9.1
590	61.3 ± 2.2	15.4 ± 0.5	3.0	90	27.7 ± 2.8	18.0 ± 0.4	3.0	131	- 9.7
610	67.8 ± 2.2	17.5 ± 0.4	3.7	104	27.5 ± 2.5	20.8 ± 0.4	3.7	107	-10.3
630	71.6 ± 2.2	19.8 ± 0.4	4.5	139	28.3 ± 2.4	22.6 ± 0.5	4.5	139	-10.9
650	74.0 ± 2.3	24.2 ± 0.4	4.5	140	34.1 ± 2.6	26.5 ± 0.5	4.5	139	-11.5
670	67.3 ± 3.7	31.0 ± 0.4	4.5	98	47.8 ± 3.0	31.8 ± 0.5	4.5	99	-12.2
690	76.9 ± 2.9	36.9 ± 0.5	4.5	126	45.6 ± 2.4	38.2 ± 0.5	4.5	126	-12.8
710	80.6 ± 3.0	43.6 ± 0.5	4.5	141	54.4 ± 3.4	44.2 ± 0.6	4.5	146	-13.4
730	87.5 ± 3.3	56.5 ± 0.6	4.5	112	59.6 ± 3.3	57.2 ± 0.8	4.5	117	-14.0
750	89.0 ± 5.3	70.0 ± 1.2	4.5	149	72.7 ± 8.8	70.4 ± 1.5	4.5	150	-14.7
770									
790	83.8 ± 3.2	106.1 ± 1.7	4.5	134	113.2 ± 3.5	102.5 ± 1.8	4.5	140	-15.9
810	94.5 ± 4.3	118.6 ± 0.9	4.5	131	105.2 ± 5.8	117.5 ± 0.9	4.5	136	-16.5
830	90.3 ± 2.9	127.7 ± 0.8	4.5	133	122.2 ± 4.0	127.3 ± 1.3	4.5	134	-17.2
850	93.5 ± 3.1	135.0 ± 0.7	4.5	96	131.3 ± 3.0	133.8 ± 0.9	4.5	95	-17.8
870	89.2 ± 2.7	137.2 ± 0.6	4.5	110	140.7 ± 2.4	134.1 ± 0.8	4.5	112	-18.4
890	99.8 ± 4.1	143.6 ± 0.6	4.5	102	137.1 ± 2.4	141.5 ± 0.8	4.5	104	-19.1
910	99.1 ± 4.1	147.4 ± 1.1	3.4 ± 0.7	234	144.7 ± 2.6	145.2 ± 1.1	2.6 ± 0.7	235	-19.4
930	105.6 ± 2.5	151.7 ± 0.5	4.0 ± 0.5	256	132.5 ± 3.9	149.7 ± 0.5	5.3 ± 0.6	256	-20.0
950	108.7 ± 5.0	152.8 ± 1.1	3.7 ± 0.8	282	137.5 ± 4.2	150.6 ± 1.0	4.5 ± 0.7	278	-20.5
970	112.4 ± 10.0	156.3 ± 1.2	6.1 ± 1.2	183	143.3 ± 3.3	153.8 ± 0.9	6.5 ± 0.6	175	-20.9

TABLE II : $\pi\pi$ phase shifts, δ^I_L in degrees determined from $\pi^- p \to \pi^- \pi^+ n$ data at 17.2 GeV/c in 20 MeV $\pi\pi$ mass bins. In each mass bin below 900 MeV six moments were fitted at 20 t values ($0.0025 < -t < 0.2$ GeV^2). Above 900 MeV, 15 moments were used at the 20 t values. The $\pi^o\pi^o$ mass distribution selects Solution 1 as the physical solution.

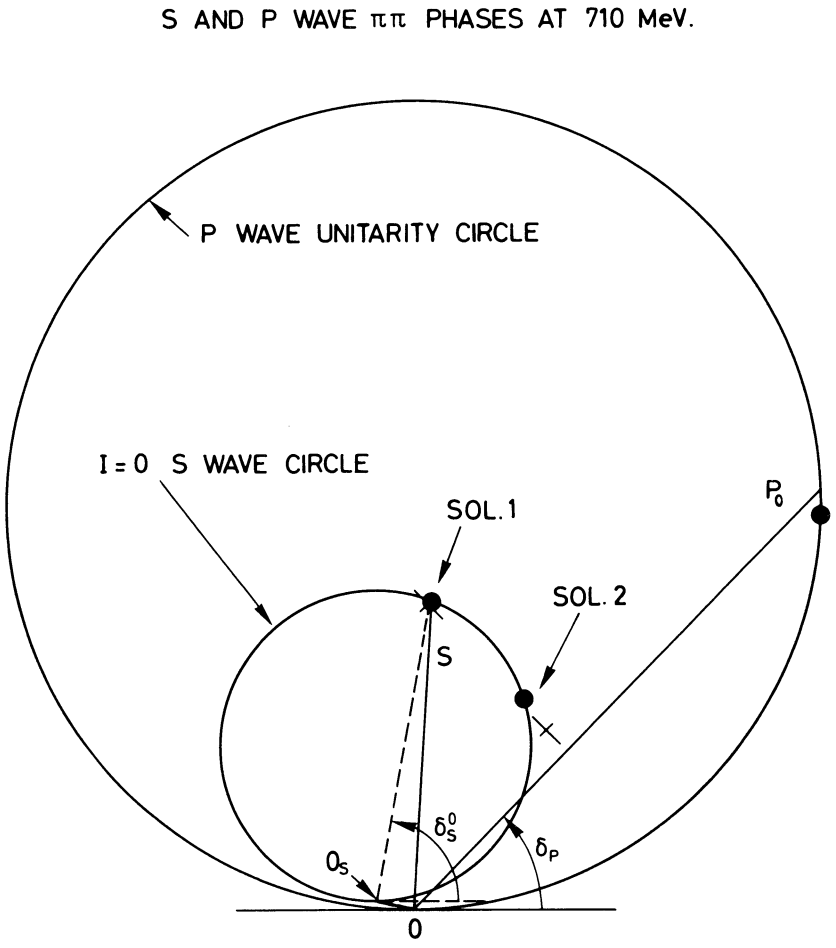

Figure 5 The S and P wave ππ phases at $M_{\pi\pi} = 710$ MeV obtained by extrapolating the amplitude solutions of Fig. 4. The scale of the unitarity circles ($1 : 2/3\sqrt{3}$) represents the relative size of the amplitudes in the production process. The length OO_S is the input I = 2 S wave. The crosses are the S wave results obtained from the dashed lines of Fig. 4. The black dots are the results of the parametric fit with elastic unitarity imposed.

The shift of origin from O to O_S is due to the input I = 2 S wave amplitude f^2_S. Knowing $S^{\parallel}/P_o$ and $S^{\perp}/P_o$ we may plot the S wave amplitude on Fig. 5. The two solutions are indicated by crosses which represent their error bars. If the S wave is elastic, as we expect, then the cross representing the physical solution should lie on the unitarity circle. We notice that the well determined component $S^{\parallel}$ is similar for the two solutions, whereas the poorly known component $S^{\perp}$ distinguishes the two solutions. It is apparent that it is not going to be easy to select the physical solution for δ^o_S simply from an analysis of $\pi^-p \to \pi^-\pi^+n$ data alone. As in previous analyses [3,5,22-24] we will have to take care to keep track of both solutions as a function of $M_{\pi\pi}$. Essentially the M = 0 moments determine $|P_o|$, $S^{\parallel}$ and $|S|^2 + |P_o|^2$ and so the best chance of getting a unique δ^o_S appears to be in a region away from the ρ where $|S|$ is significantly different for the two solutions and leads to different extrapolated cross-sections. The inclusion of the $M \neq 0$ moments is necessary to allow a reliable determination of P_o and S. Moreover, in principle, from a knowledge of the sign of $P^{\perp}_{-}$, they also allow the sign of $S^{\perp}$ to be determined (cf. $< Y^1_1 >$). In practice $P^{\perp}_{-}$ is small and poorly determined and so is not decisive.

So far S wave unitarity has not been imposed. At first sight it appears that this could select the physical solution - perhaps one solution is always nearer to the circle than the other solution. However, $S^{\perp}$, like $P^{\perp}_{-}$, is badly determined and it would be misleading to select the solution in this way. Rather at the outset we should impose unitarity (at $t = \mu^2$) on the analysis and then see if one solution is preferred to the other. We describe such an analysis below.

5. $\pi\pi$ PHASE SHIFT ANALYSIS FOR $M_{\pi\pi}$ BELOW 1 GeV

The analysis is based on the high statistics $\pi^-p \to \pi^-\pi^+n$ data obtained[4] at a laboratory momentum of 17.2 GeV/c. S channel moments of the $\pi^-\pi^+$ angular distribution are used in 20 MeV $\pi\pi$ mass bins from $M_{\pi\pi} = 440$ MeV upwards. In each mass bin we determine the structure of the production amplitudes in the range $0 < -t < 0.2$ GeV^2 by fitting the moments to parametric forms based on Eqs. (13). For the results that we present, the slopes of the π, C, A_2 contributions, the complex $C(\mu^2)$, and g^F_A of Eqs. (13) are taken as parameters in each $M_{\pi\pi}$ bin, in addition to δ^o_S and δ_P ; the signature factors $_i$ are included and $g^{NF}_A = 0.25\, g^F_A$. We include D waves as outlined in Section 4. We impose elastic unitarity, $f_L = \sin\delta_L\, e^{i\delta_L}$, through Eqs. (14)-(16), except that, above the onset of the $\pi\omega$ channel, $M_{\pi\pi} = 920$ MeV, we allow the P wave to be inelastic.

The unitarity constraint is only true at $t = \mu^2$. However, we included a term $[1 + a(t - \mu^2)]$ on the right-hand side of Eq. (16). Since the unitarity phase is preserved[25] we took the parameter a to be real. Such a term could also arise from differing amounts of absorption in the π pole contributions to S and P_o, or from a t dependence associated with crossing from the t to the s channel. The values found for the parameter a in the different mass bins were distributed about zero, and typically $a \approx \pm 0.5$ GeV^2. The results we present have $a = 0$. Values of $a = \pm 0.5$ lead to changes in δ_s^o and δ_p of about $\pm 2^o$ and $\pm 0.5^o$, respectively.

We tried several different forms of amplitude parametrization based on Eqs. (13), allowing different slope factors $\exp[b(t - \mu^2)]$ on individual contributions, using different input values of g_A^F/g_A^{NF}, etc. The phase shift results were extremely stable to such changes of parametrization. We also repeated the analysis using only data for $-t < 0.1$. Again the results were essentially unaltered. The curves shown in Fig. 4 are the form of the amplitudes at 710 MeV. We see that they are a good description of the amplitude components determined t by t indicating that the chosen parametric form is adequate. The fit to the observed s channel moments is shown in Fig. 6.

a) S and P wave $\pi\pi$ phases :

The phase shifts obtained by the method outlined above are shown in Fig. 7 and listed in Table II. There are two solutions mainly differing in the values of δ_s^o. Solution 1 is characterized by a small P_-^1 and solution 2 by a small S^1. By this means or by following the Barrelet zeros (see Section 7, Fig. 16) it is possible to keep track of the two solutions through the ρ mass region. The solutions are stable to changes of parametrization and to changes of the t region over which the data are fitted. With the exception of solution 2 below $M_{\pi\pi} = 650$ MeV, the solutions are also stable to reasonable variations of the input values of δ_s^2 and δ_D^o. The black dots and open circles of Fig. 7 denote solutions 1 and 2 respectively. For comparison we show by a dashed curve the solution obtained by Protopopescu et al.[24] from an analysis of $\pi^+p \to \pi^+\pi^-\Delta^{++}$ data.

In contrast to recent analyses[6,22,24], we obtain two acceptable solutions below (as well as above) the ρ mass. At low $M_{\pi\pi}$ the solutions have very different $|S|$, and therefore lead to different extrapolated $\pi\pi$ cross-sections. However, both values are compatible with the physical region data since the non π exchange background differs for the two solutions in such a way as to give good fits to the data in each case. We discuss this further in the next section.

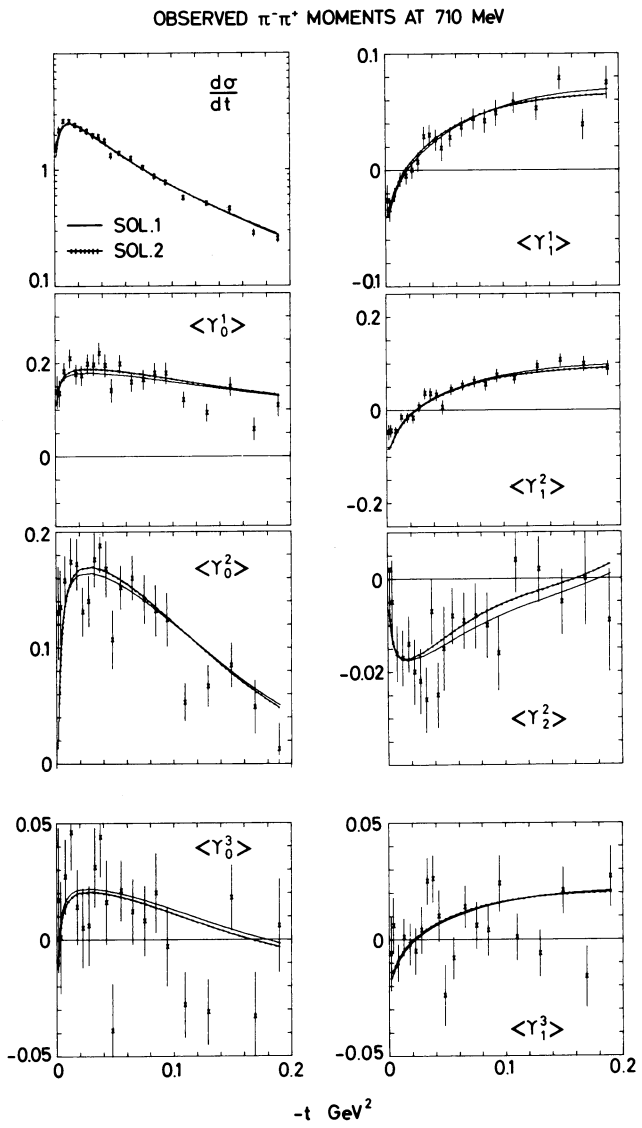

Figure 6 The fits to the s channel moments with $J \leq 2$ at $M_{\pi\pi} = 710$ MeV corresponding to solutions 1 and 2 of Table II. The description of the $J = 3$ moments is also shown ($\delta^0_D = 4.5^0$).

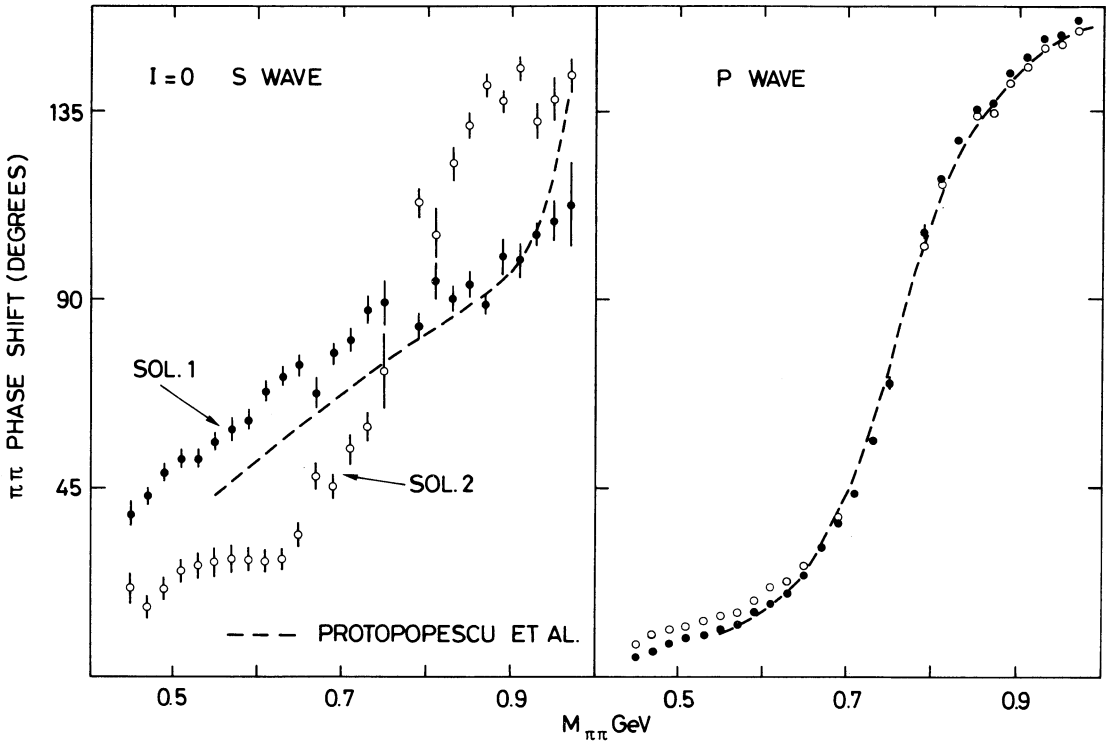

Figure 7 The S and P wave ππ phase shifts, δ_S and δ_P, below 1 GeV determined from the $\pi^-p \to \pi^-\pi^+n$ amplitudes. The values are listed in Table II. Solution 1 is the physical solution. For comparison the dashed line is the favoured solution obtained by Protopopescu et al.[24].

If we were to believe that the non-vanishing absorptive background $[C(t)$ of Eq. (13)$]$ is dominantly real relative to π exchange then this appears to favour the solution with the smaller $P_-^\perp$, that is, solution 1. On the other hand, although the results of the phase coherent analysis $(P_-^\perp = 0)$ described in the next section do in general prefer solution 1, we find even there an acceptable solution 2 at $M_{\pi\pi}$ values below and above the ρ mass region. From the analysis above it is clear that the $\pi^-\pi^+n$ data alone do not resolve the S wave ambiguity in the elastic region.

The most direct way to select the physical solution is to study the $\pi^o\pi^o$ mass distribution[26,27], since here only even L ππ partial waves can contribute. The histogram in Fig. 8 is the $\pi^o\pi^o$ mass spectrum for $2\mu^2 < -t < 8\mu^2$ obtained from a $\pi^-p \to \pi^o\pi^o n$ experiment[26] at 8 GeV/c. In terms of ππ phase shifts this spectrum is, to a good approximation, proportional to

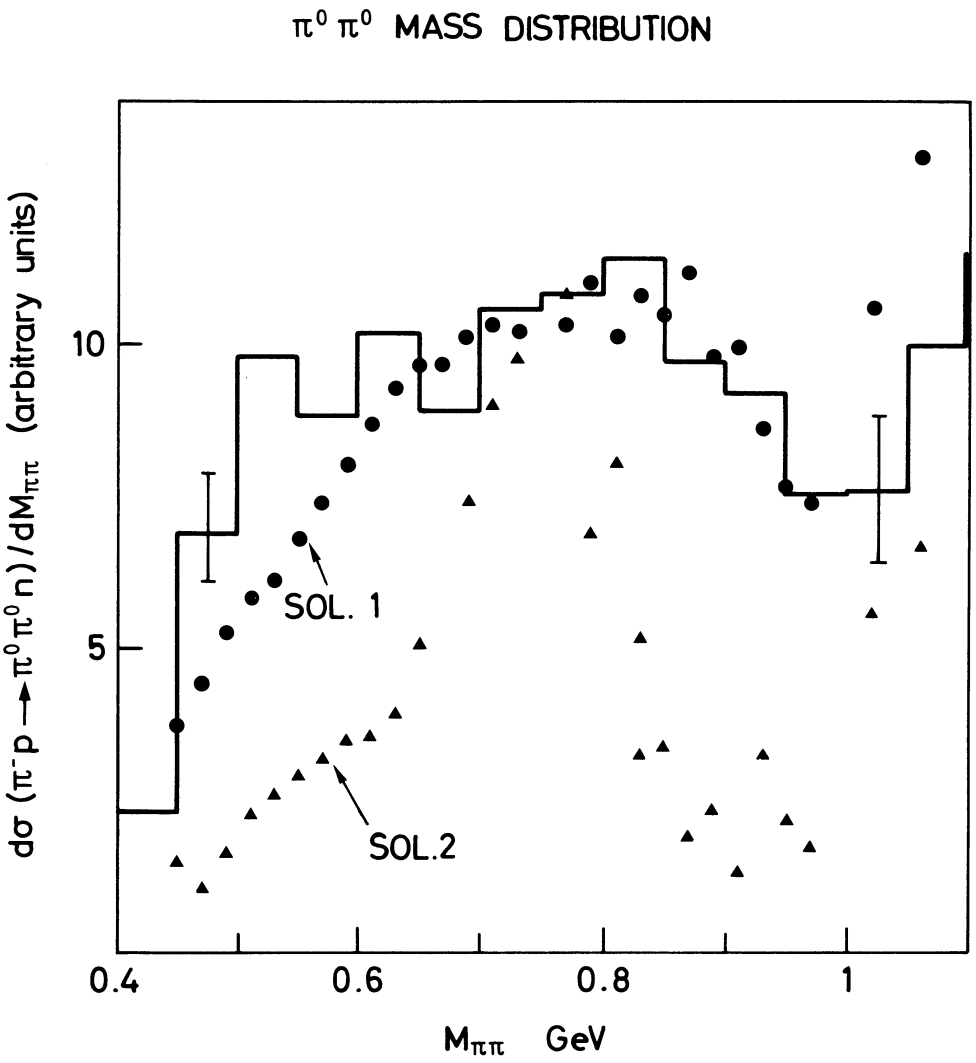

Figure 8 The histogram is the $\pi^o\pi^o$ mass spectrum for $2\mu^2 < -t < 8\mu^2$ from $\pi^- p \to \pi^o\pi^o n$ at 8 GeV/c[26]. The circles (triangles) are the shape of the spectrum calculated from the $\pi\pi$ phases of solution 1 (solution 2) respectively. The scale is arbitrary.

$$\frac{d\sigma(\pi^0\pi^0)}{dM_{\pi\pi}} \propto \frac{M_{\pi\pi}^2}{q} \sum_{L=0,2} (2L+1) \left| \tfrac{1}{3} f_L^0 - \tfrac{1}{3} f_L^2 \right|^2$$

where the partial wave amplitudes f_L^I, are defined as in Eq. (6). The predictions of the two solutions are shown on the figure. A comparison of the shapes of the mass spectrum clearly selects solution 1 as the physical solution.

Above $M_{\pi\pi} = 920$ MeV we allow the P wave to be inelastic. Although $|f_P|$ is well determined, the inelasticity parameter η_P is poorly constrained by the data for $M_{\pi\pi} \sim 950$ MeV. The reason is apparent from Fig. 9. The data determine $|f_P|$, $|f_S|$ and $\cos(\delta_S - \delta_P)$ but not the over-all phase, and thus the solutions shown have comparable χ^2. The phase shifts listed assume that the P wave is elastic below 1 GeV.

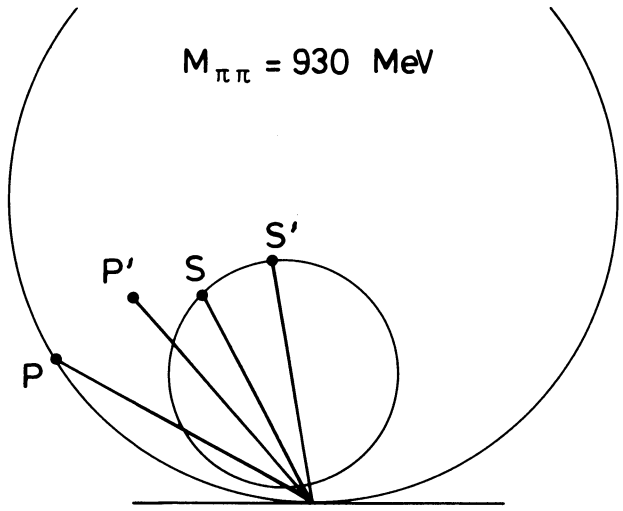

Figure 9 S, P denote solution 1 at $M_{\pi\pi} = 930$ MeV. The solution S', P', with an inelastic P wave gives a comparable fit to the data.

To determine resonance parameters we use the form[28]

$$f_L = \frac{\alpha M_R \Gamma}{M_R^2 - M_{\pi\pi}^2 - i M_R \Gamma}, \qquad (17)$$

with

$$\Gamma = \left(\frac{q}{q_R}\right)^{2L+1} \frac{D_L(q_R r)}{D_L(q r)} \Gamma_R$$

For the ρ we use $D_1(y) = 1 + y$ and fit to the P wave phase shift of solution 1 in the range $650 \leq M_{\pi\pi\pi} \leq 890$ MeV. With this parametrization, we find for the ρ

$$M_\rho = 772.2 \pm 0.6 \text{ MeV}, \qquad \Gamma_\rho = 143.1 \pm 1.1 \text{ MeV},$$

$$r_\rho = 0.83 \pm 0.08 \text{ f}.$$

b) D wave in the elastic region :

In the ρ mass region the observed s channel $\langle Y_0^3 \rangle$ moment has a systematic behaviour versus both $M_{\pi\pi\pi}$ and t which is consistent with P-D interference. For a fixed $t \sim -0.05$ GeV^2, the normalized $\langle Y_0^3 \rangle$ moment decreases from around 0.04 for $M_{\pi\pi\pi} \sim 600$ MeV, through zero in the region of the ρ mass, to about -0.03 for $M_{\pi\pi\pi} \sim 900$ MeV. For fixed $M_{\pi\pi\pi}$, $\langle Y_0^3 \rangle$ reaches a maximum size for $-t \sim 0.05$ and then decreases, changing sign for $-t \sim 0.15$ GeV^2. Examples of the observed s channel $\langle Y_0^3 \rangle$ moment are shown in Fig. 10.

In terms of production amplitudes

$$\sqrt{4\pi}\, N \langle Y_0^3 \rangle = \frac{6}{\sqrt{35}} \operatorname{Re}\left(\sqrt{3}\, P_0 D_0^* - P_- D_{1-}^* - P_+ D_{1+}^*\right)$$

$$\simeq \frac{6\sqrt{3}}{\sqrt{35}} \left|\frac{D_0}{P_0}\right| \left[|P_0|^2 - |P_-|^2 - |P_+|^2\right] \cos(\delta_P - \delta_D). \qquad (18)$$

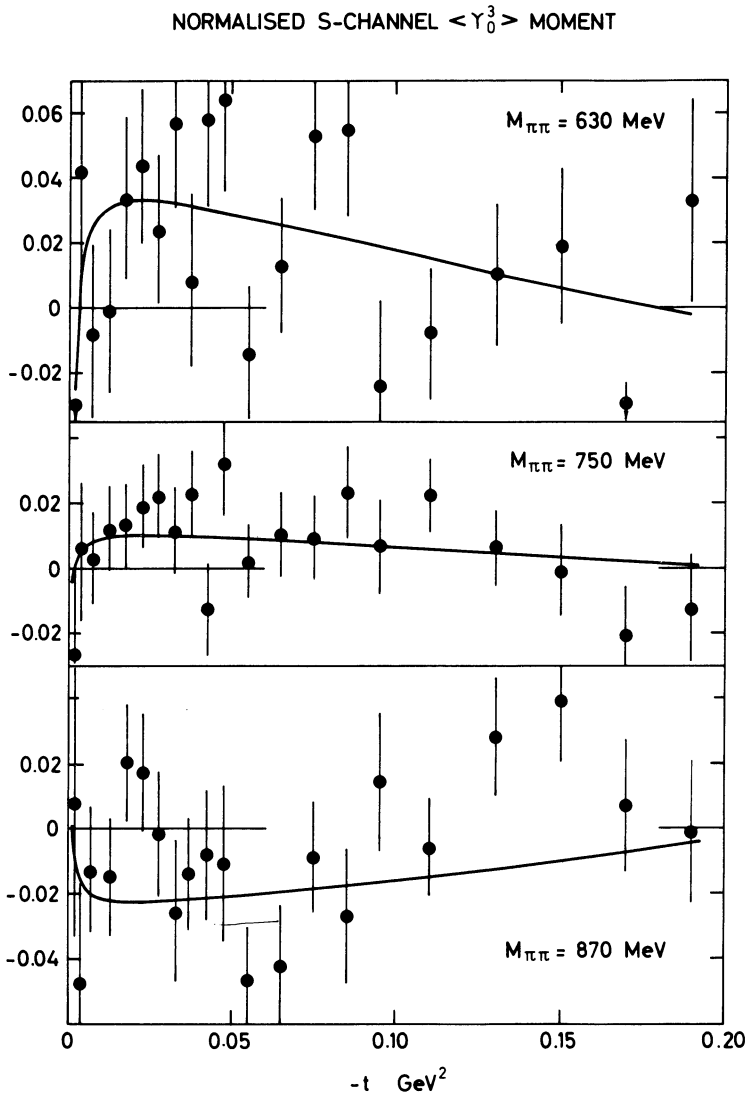

Figure 10 The t dependence of the s channel $< Y_0^3 >$ moment in three typical 20 MeV $M_{\pi\pi}$ bins. The curves are the description of the data for $\delta_D^0 = 4.5^0$.

The last equality is obtained assuming the proportionality relation

$$D_{1\pm} = \sqrt{3}\ D_0 (P_\pm / P_0), \qquad (19)$$

where the $\sqrt{3}$ arises from crossing the π exchange contribution to the s channel. For instance such a relation is implied by the Williams model. In Eq. (18) the $M_{\pi\pi\pi}$ behaviour of $< Y_0^3 >$ arises mainly from the factor $\cos(\delta_P - \delta_D)$, while the t behaviour of $< Y_0^3 >$ is due to the term in square brackets.

Knowing the P wave amplitudes and taking the D wave to be elastic below $M_{\pi\pi\pi} = 900$ MeV, and dominantly $I = 0$, we calculate δ_D^0 for each $M_{\pi\pi\pi}$ bin by comparing Eq. (18) with the $< Y_0^3 >$ data. Over the entire range 620 MeV $< M_{\pi\pi\pi} <$ 900 MeV we find δ_D^0 is essentially constant with a value of $\delta_D^0 = 4.5^\circ$. For mass values close to $M_{\pi\pi\pi} = 780$ MeV δ_D^0 cannot be reliably determined since the P and D amplitudes are about $\pi/2$ out of phase. That δ_D^0 should be so large for $M_{\pi\pi\pi} \sim 650$ MeV is puzzling. The curves in Fig. 10 are calculated from Eq. (18) using $\delta_D^0 = 4.5^\circ$. Equation (18) gives a good (one parameter) description of the t and $M_{\pi\pi\pi}$ behaviour of the $< Y_0^3 >$ moment. Versus $M_{\pi\pi\pi}$ it predicts a $< Y_0^3 >$ sign change at $M_{\pi\pi\pi} \sim 780$ MeV (the data crossover is at $M_{\pi\pi\pi} \sim 800$ MeV) and versus t a sign change at $-t \sim 0.2$ (compared to 0.15 in the data).

In the S and P wave analysis in the region 620 $< M_{\pi\pi\pi} <$ 900 MeV we took $\delta_D^0 = 4.5^\circ$. Below 620 MeV the estimates of δ_D^0 may not be reliable, since for $M_{\pi\pi\pi} \lesssim 500$ MeV an anomalous behaviour is observed in some higher moments[4] and, therefore, we assumed a q^5 threshold behaviour of δ_D^0. For $M_{\pi\pi\pi} >$ 900 MeV we included the $J = 3,4$ moments and determined $\delta_D^{0\,\pi\pi\pi}$ in each mass bin.

6. PHASE COHERENT ANALYSIS

We repeated the $\pi\pi$ phase shift analysis using essentially a Williams' model parametrization of the production amplitudes. In place of Eqs. (13) we use the simplified forms

$$P_0 = -\frac{g_\pi}{\sqrt{q}} M_{\pi\pi} \frac{\sqrt{-t'}}{t-\mu^2} e^{b(t-\mu^2)}$$

$$P_- = \frac{g_\pi}{\sqrt{q}} \left[\frac{2t'}{t-\mu^2} - C \right] e^{b(t-\mu^2)} \qquad (20)$$

$$P_+ = -\frac{g_\pi}{\sqrt{q}} C e^{b(t-\mu^2)}$$

where C, which specifies the absorptive background, is assumed to be real and independent of t. Strictly speaking the Williams' model has C = 1, however, here we take C as a parameter to be determined in each mass bin. Departures from the above simple parametrization occur for $-t \gtrsim 0.15$ GeV^2 due to the neglect of A_2 exchange contributions, etc.[15,4]. Therefore we restrict the analysis to the data in the region $-t < 0.1$ GeV^2. The points shown in Fig. 11 for $M_{\pi\pi} < 1$ GeV are the results of this analysis. The values of δ_S^0 are in excellent agreement with solution 1 of Section 5 and are a demonstration of the stability of the phase shifts to a change of parametrization.

Since phase coherence between P_0 and P_- is an input assumption here, it is not surprising that we obtain solution 1. However, for mass bins where the two solutions of Section 5 are dissimilar (i.e., away from the region of the ρ mass) we also find solution 2, and with comparable χ^2. Moreover the values of C are almost identical for the two solutions, whereas for $M_{\pi\pi} \sim 500$ MeV we have already remarked (cf. Section 5) that the background has to be different for the two solutions. This apparent contradiction is resolved when we note that δ_P is significantly different for the two solutions in this mass region.

7. PHASE SHIFT ANALYSIS IN THE INELASTIC REGION

Above the $K\bar{K}$ threshold we cannot impose elastic unitarity. Indeed, the $\pi\pi \to K\bar{K}$ cross-section is observed[24,29] to rise rapidly to its S wave unitarity limit. Further we can no longer regard the D wave as a small correction. On the other hand we still want to perform a phase shift analysis at each $M_{\pi\pi}$ independently. We use a similar method to that described in Sections 4 and 5.

a) Production amplitude analysis :

From the observed s channel moments with $J, M \leq 4$ we determine the production amplitudes $L_{\lambda\pm}$ with $L, \lambda \leq 2$, and extrapolate S, P_0, D_0 to the π exchange pole. The data determine the magnitudes and relative phases of S, P_0, D_0, but not the over-all phase. In the elastic region unitarity determined the over-all phase, but in the inelastic region the unitarity constraint is weaker. For example a solution, such as shown in Fig. 12, can be rotated through any angle provided that the partial waves lie within their unitarity circles.

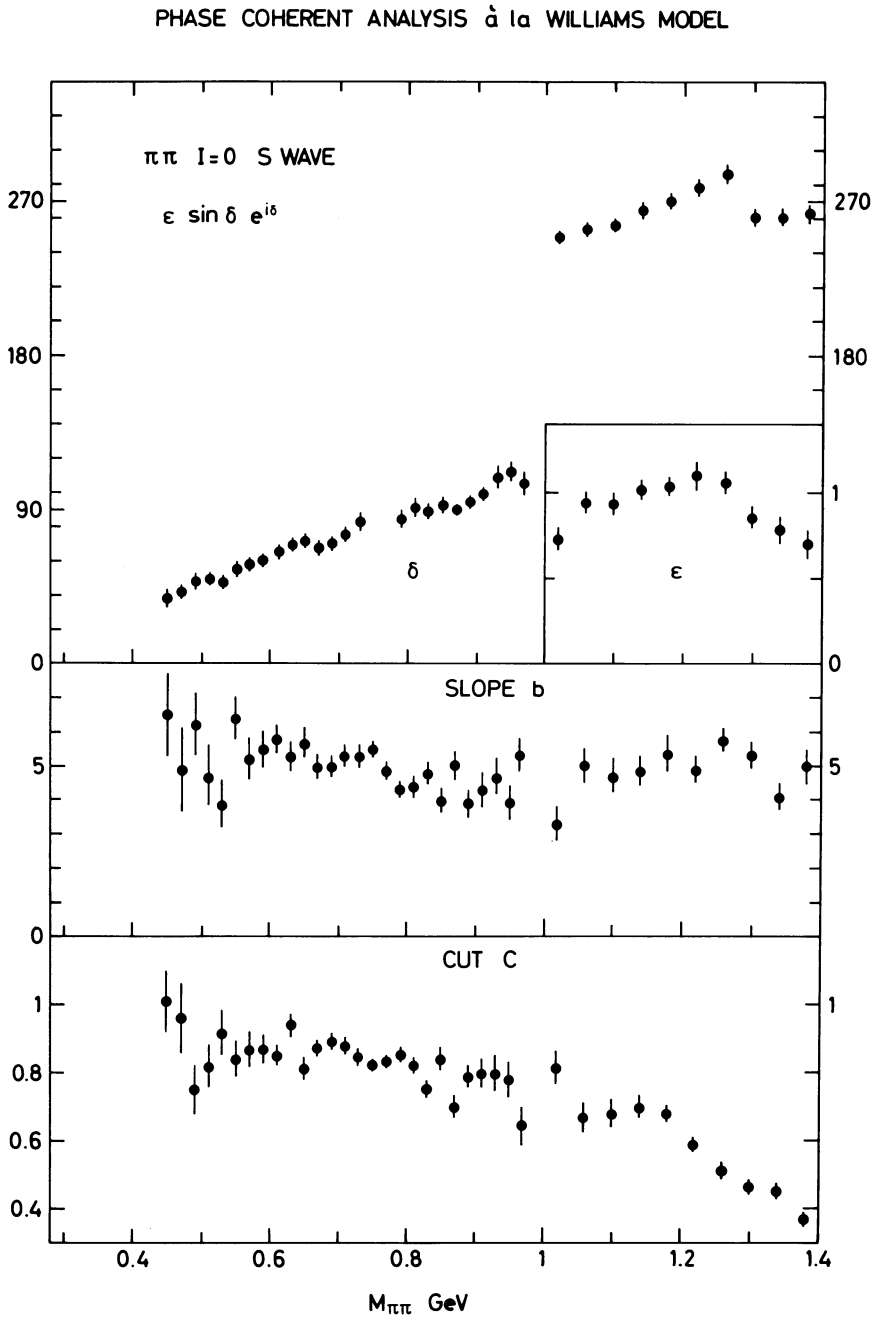

Figure 11 Some results of a phase shift analysis using a simplified parametrization, Eqs. (20). The results above 1 GeV are discussed in Section 7.d.

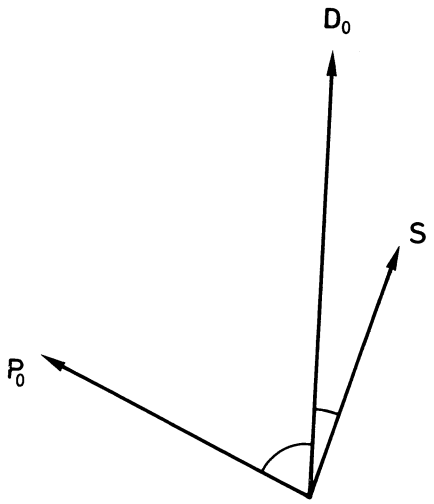

Figure 12 Dominant π exchange amplitudes. Only the magnitudes and relative phases are determined.

We have tried several different forms of parametrization of the s channel amplitudes. As in the elastic region we find that, as long as we include the $\lambda \neq 0$ amplitudes, the phase shifts are stable to changes of the form of the parametrization and to changes of the t interval over which the moments are fitted. The results we present use the parametrization of Eqs. (13), as stated in Section 5, with the additional assumptions

$$D_{1\pm} = \sqrt{3}\, P_{\pm}\, \frac{D_0}{P_0} \tag{21}$$

$$D_{2\pm} = \frac{\sqrt{-t'}}{M_{\pi\pi}}\, D_{1\pm}\,, \tag{22}$$

which are motivated by studying the t to s channel crossing matrix. Equations (21) and (22) are correct provided the main contribution to the s channel $\lambda = 1,2$ amplitudes is due to π exchange and its absorptive correction. This is expected to be a good approximation for $-t < 0.2$ GeV^2, particularly as A_2 exchange decreases* relative to π exchange with increasing $M_{\pi\pi}$.

---

* For instance, for $-t \gtrsim 0.4$ GeV^2 the moments indicate that the natural parity exchange contribution is less dominant in the f region than in the ρ region.

In the region $1.0 < M_{\pi\pi} < 1.4$ GeV we used data in 40 MeV mass bins. In each mass bin we fitted the s channel moments with $J \leq 4$ in the interval $0.005 < -t < 0.2$ GeV^2. A typical fit is shown in Fig. 13. The two solutions have comparable χ^2 but have different magnitudes and relative phases of S, P_o and D_o. We parametrize the partial wave amplitudes, f_L of Eq. (4) in the form

$$f_L = \begin{cases} r_L e^{i\delta_L} & \text{for } L=1 \\ \frac{2}{3} r_L e^{i\delta_L} & \text{for } L=0,2 \end{cases} \qquad (23)$$

and fix the over-all phase by the choice $\delta_D = 90^\circ$. The 2/3 is inserted for even L so that, if there were no $I=2$ $\pi\pi$ amplitude, unitarity would require $r_L \leq \sin\delta_L$. This bound is not imposed in the fit to the data. The results for each 40 MeV mass bin are listed in Table III. In Fig. 14 they are shown in the form $\sqrt{2L+1}\, f_L$, which represents their relative strength in the production process. We must now explain why we have shown two solutions.

b) Zero contours :

In addition to the continuum ambiguity of the over-all phase, are there discrete ambiguities in the phase shift analysis ? Yes, for S, P, D waves there are four solutions giving identical $d\sigma_{\pi\pi}/d\Omega$. A useful way[30,31] of seeing this and of keeping track of the four solutions is to study the zeros of the $\pi^+\pi^-$ scattering amplitude in the complex $z \equiv \cos\theta_{\pi\pi}$ plane. These have been called Barrelet zeros[32]. For S, P, D waves the $\pi\pi$ amplitude, $A(z)$, will have two such zeros, say at $z = z_1$ and $z = z_2$. Thus

$$\frac{d\sigma_{\pi\pi}}{d\Omega} = A(z)\, A^*(z^*) = c(z-z_1)(z-z_2)(z-z_1^*)(z-z_2^*), \qquad (24)$$

and for each z_i there is a twofold ambiguity. Is $z = z_i$ or $z = z_i^*$ the zero of A ? For example, at $M_{\pi\pi} = 1.18$ GeV from solution 1 of Fig. 15 we calculate the zeros and predict the other three solutions that are shown. Having obtained one solution the procedure is to use these three predictions as starting values in the analysis of the observed moments. In this way we obtain four solutions at each $M_{\pi\pi}$. Two of the solutions (those denoted solutions 3 and 4 in the example shown in Fig. 15) are clearly ruled out by studying continuity of the partial waves with $M_{\pi\pi}$. The real and imaginary parts of the positions of the zeros for the other two solutions are shown in Fig. 16. By following the zero contours we can keep track of the solutions. However, two similar

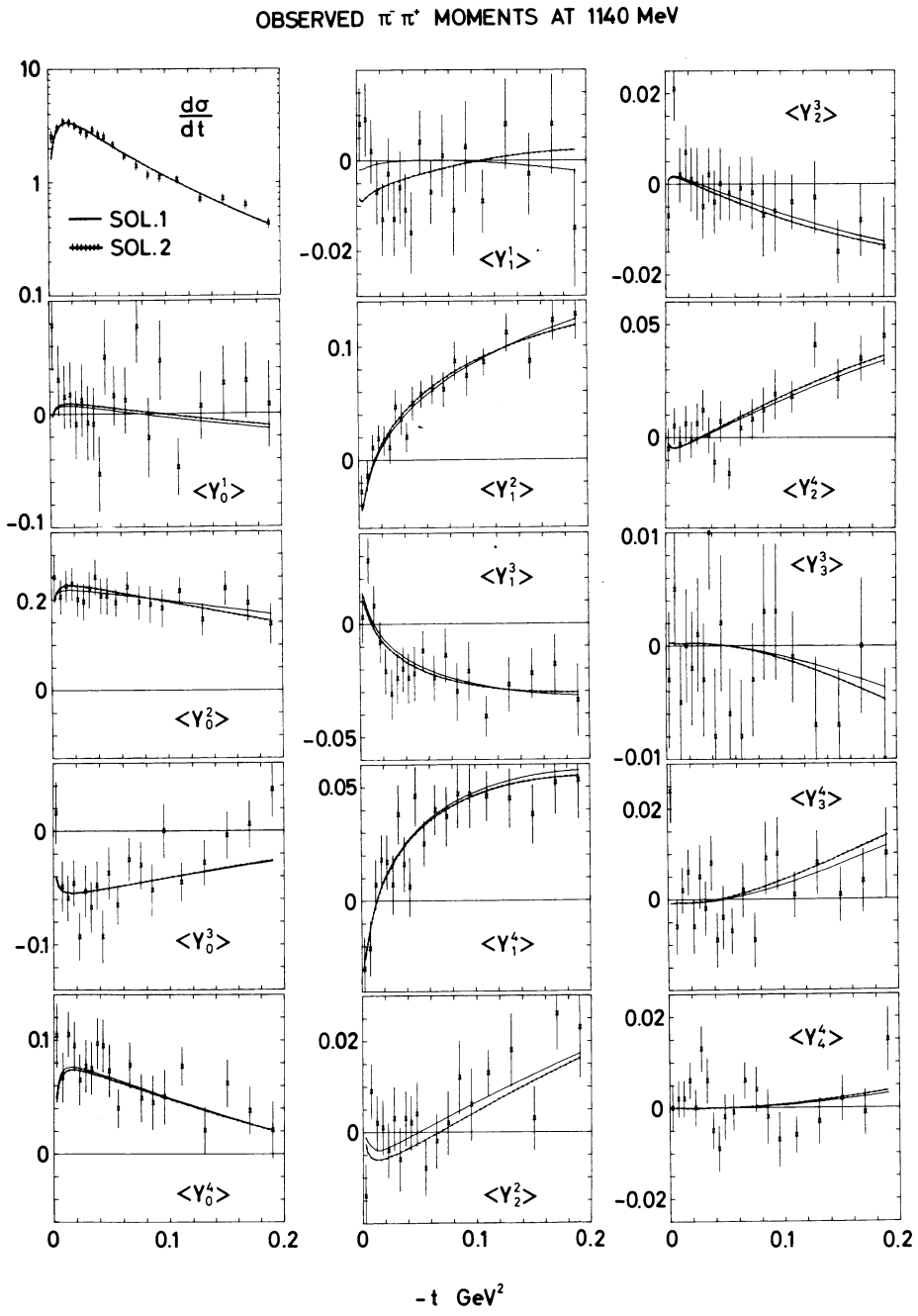

Figure 13 The fits to the s channel moments in a typical mass bin, $1.12 < M_{\pi\pi} < 1.16$ GeV. The partial wave parameters are given in Table III.

$M_{\pi\pi}$ (GeV)	Solution 1						Solution 2					
	η_S	δ_S	η_P	δ_P	η_D	χ^2	η_S	δ_S	η_P	δ_P	η_D	χ^2
1.02	0.74 ± 0.10	146 ± 2	0.32 ± 0.02	212 ± 2	0.21 ± 0.02	324	0.16 ± 0.03	193 ± 24	0.42 ± 0.01	201 ± 2	0.21 ± 0.02	327
1.06	0.81 ± 0.08	146 ± 2	0.33 ± 0.02	213 ± 2	0.24 ± 0.02	286	0.22 ± 0.05	190 ± 22	0.45 ± 0.01	203 ± 2	0.24 ± 0.02	296
1.10	1.01 ± 0.04	149 ± 2	0.27 ± 0.01	218 ± 2	0.32 ± 0.01	348	0.28 ± 0.04	168 ± 8	0.45 ± 0.01	203 ± 2	0.32 ± 0.01	364
1.14	1.08 ± 0.05	148 ± 2	0.22 ± 0.02	211 ± 2	0.39 ± 0.01	273	0.32 ± 0.04	157 ± 5	0.45 ± 0.01	195 ± 1	0.39 ± 0.01	277
1.18	1.13 ± 0.06	145 ± 2	0.27 ± 0.03	207 ± 2	0.54 ± 0.02	268	0.62 ± 0.10	140 ± 3	0.44 ± 0.04	197 ± 2	0.54 ± 0.02	274
1.22	1.23 ± 0.06	136 ± 2	0.22 ± 0.03	195 ± 2	0.69 ± 0.01	266	0.86 ± 0.10	127 ± 4	0.40 ± 0.04	189 ± 4	0.69 ± 0.01	272
1.26	1.11 ± 0.06	121 ± 3	0.23 ± 0.03	171 ± 5	0.82 ± 0.02	353	1.21 ± 0.05	126 ± 3	0.15 ± 0.03	164 ± 6	0.81 ± 0.02	348
1.30	1.02 ± 0.06	99 ± 5	0.32 ± 0.03	163 ± 2	0.78 ± 0.02	327	1.29 ± 0.03	122 ± 3	0.10 ± 0.03	116 ± 7	0.78 ± 0.02	319
1.34	0.94 ± 0.08	83 ± 6	0.32 ± 0.03	150 ± 4	0.66 ± 0.02	292	1.17 ± 0.05	116 ± 5	0.19 ± 0.03	61 ± 14	0.66 ± 0.01	286
1.38	0.93 ± 0.09	81 ± 10	0.31 ± 0.04	144 ± 6	0.57 ± 0.02	307	1.14 ± 0.04	118 ± 5	0.20 ± 0.02	64 ± 11	0.56 ± 0.02	311

TABLE III : The $\pi\pi$ partial wave amplitudes, f_L of eqn. (23), obtained in the analysis of reaction $\pi^- p \to \pi^- \pi^+ n$ in the region $1.0 < M_{\pi\pi} < 1.4$ GeV. The over-all phase is fixed by the choice $\delta_D = 90^\circ$. In each 40 MeV mass bin we fit 15 moments at 19 t values in the range $0 < -t < 0.2$ GeV^2. Solution 1 is the physical solution.

EXTRAPOLATED S, P_0, D_0 PRODUCTION AMPLITUDES ($1.0 < M_{\pi\pi} < 1.4$ GeV)

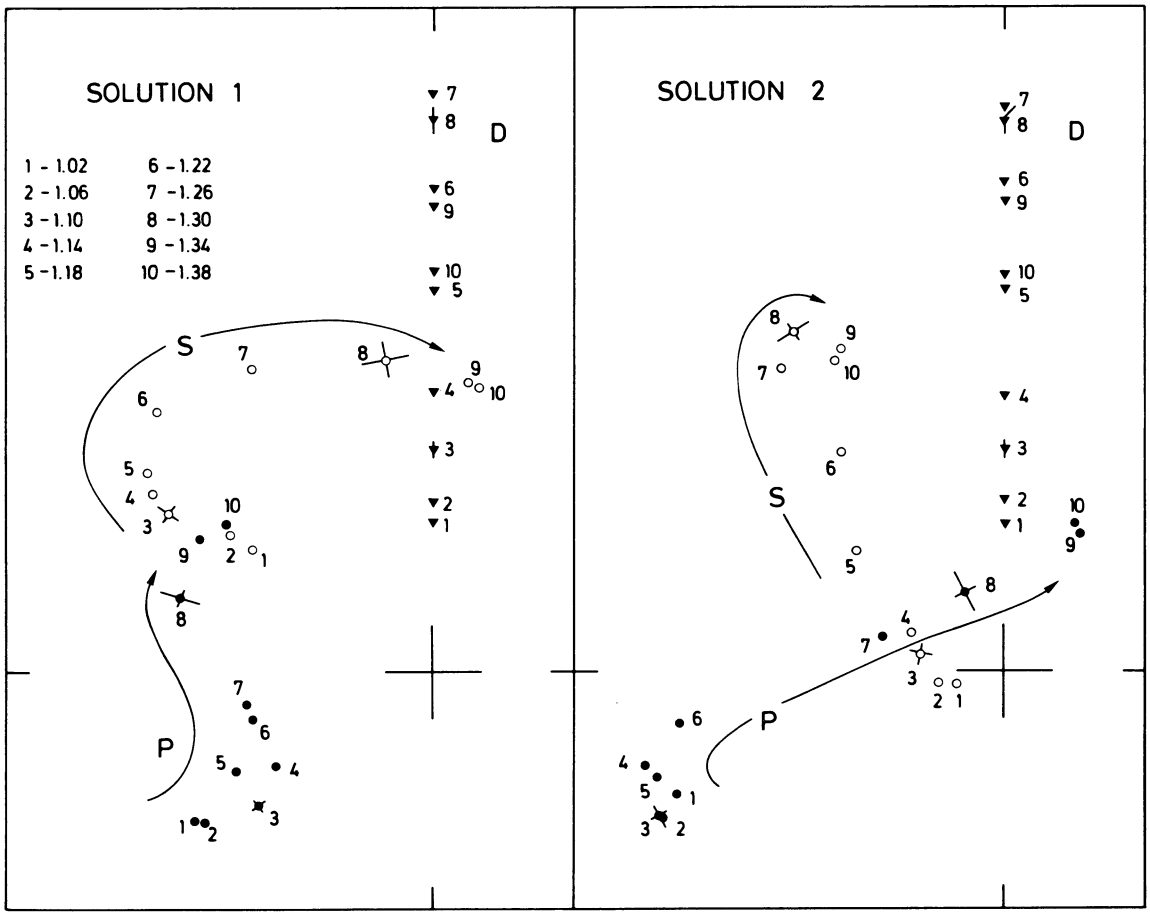

Figure 14 Two solutions for the $\pi^+\pi^-$ partial wave amplitudes f_L (scaled by $\sqrt{2L+1}$) found by analyzing $\pi^-p \to \pi^-\pi^+n$ data in 40 MeV mass bins in the range $1.0 < M_{\pi\pi} < 1.4$ GeV. We choose $\delta_D = 90^\circ$. Typical errors are shown at $M_{\pi\pi} = 1.1$ and 1.3 GeV. The results are listed in Table III.

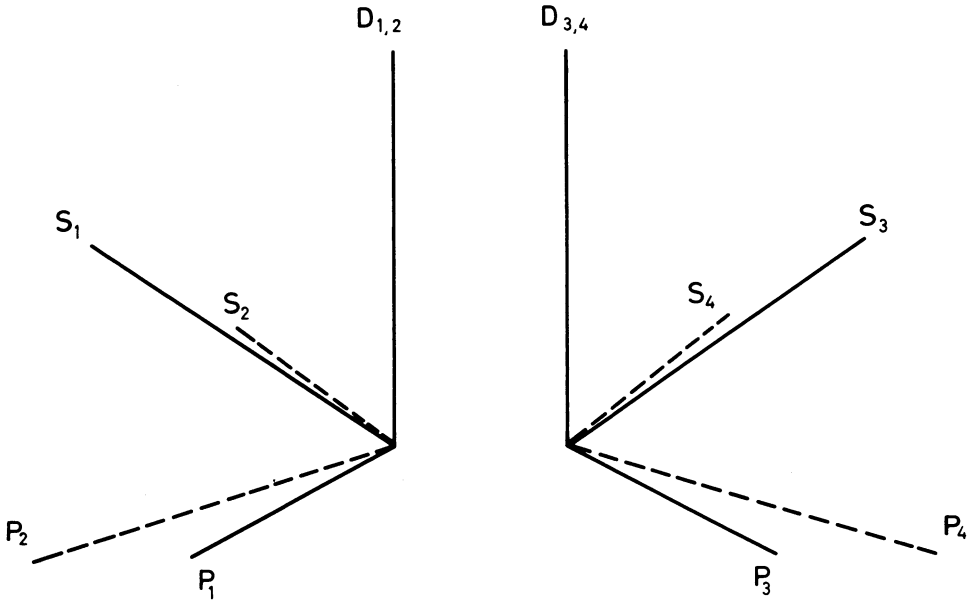

Figure 15 The four solutions at $M_{\pi\pi} = 1.18$ GeV.

solutions exist whenever Im $z_i \approx 0$. For example, for $M_{\pi\pi} \gtrsim 1.26$ GeV we have to use continuity of the zeros to decide which is solution 1 and which is solution 2. We also see that solutions 3 and 4 will need to be considered for $M_{\pi\pi} > 1.4$ GeV as Im z_2 is becoming small.

The actual solutions need not have exactly complex conjugate zeros, since, for example, the predicted absorption in the production process may differ for the solutions and so lead to a different extrapolated $\pi\pi$ cross-section, $d\sigma_{\pi\pi}/d\Omega$. Absorption decreases rapidly with increasing $M_{\pi\pi}$ and in the region above 1 GeV we do, in fact, have solutions with approximately complex conjugate zeros. In Fig. 16 we also show the positions of the zeros obtained from the phase shifts in the elastic region. The two solutions there are not, in general, due to complex conjugate zeros, but arise because the production amplitude analysis leads to different extrapolated $d\sigma_{\pi\pi}/d\Omega$. For example, at $M_{\pi\pi} \approx 600$ MeV there are two additional solutions with Im $z_1 > 0$ but with partial waves that do not satisfy unitarity.

It is illuminating to draw the contours of Re z_i on the Mandelstam plot. They are shown in Fig. 17. The continuation of the contour z_1 towards the Mandelstam triangle has been

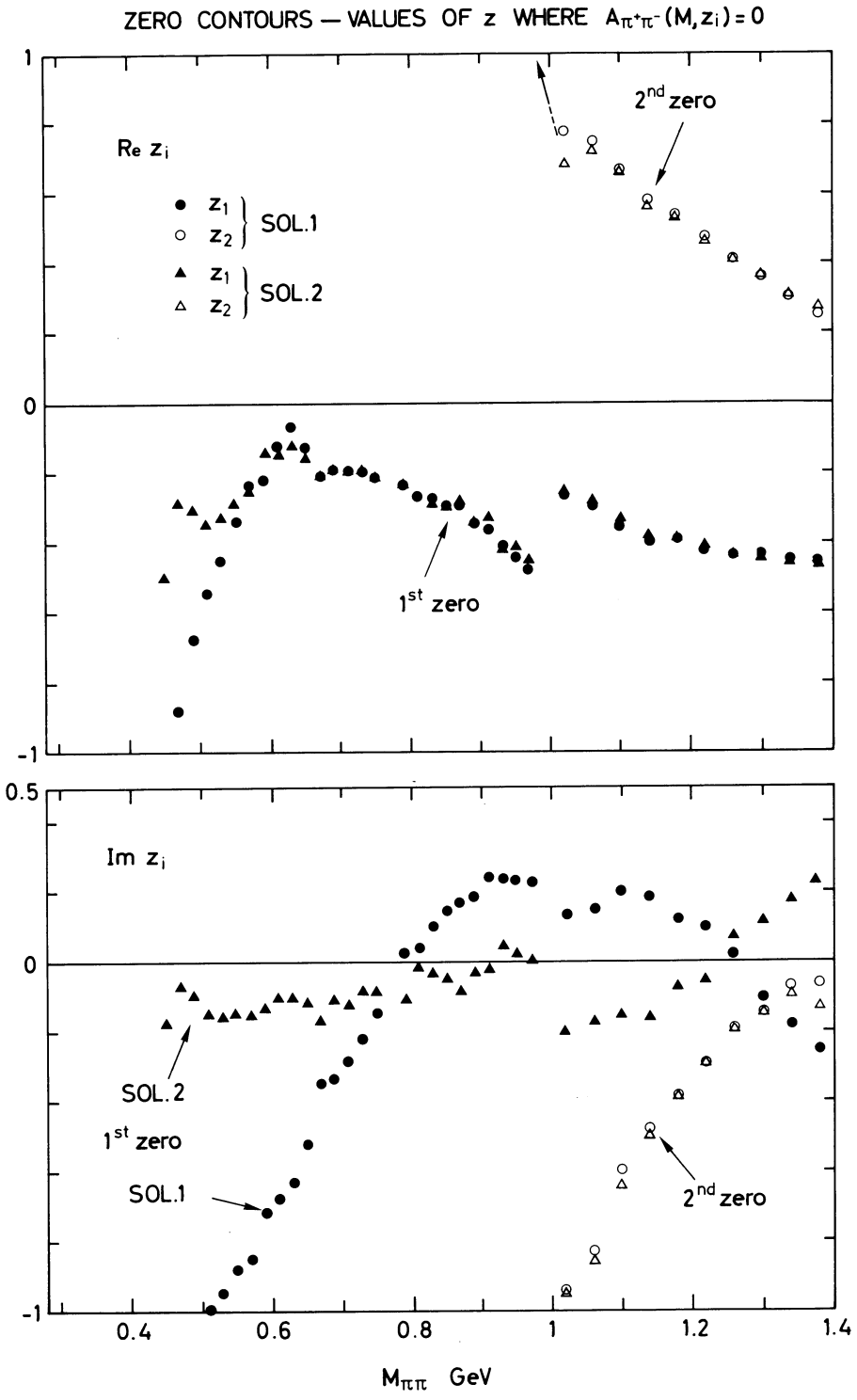

Figure 16 The positions of the zeros, $z = z_i$, of the $\pi^+\pi^-$ amplitude as calculated from the two partial wave solutions listed in Tables II and III. z is the cosine of the $\pi\pi$ c.m. scattering angle.

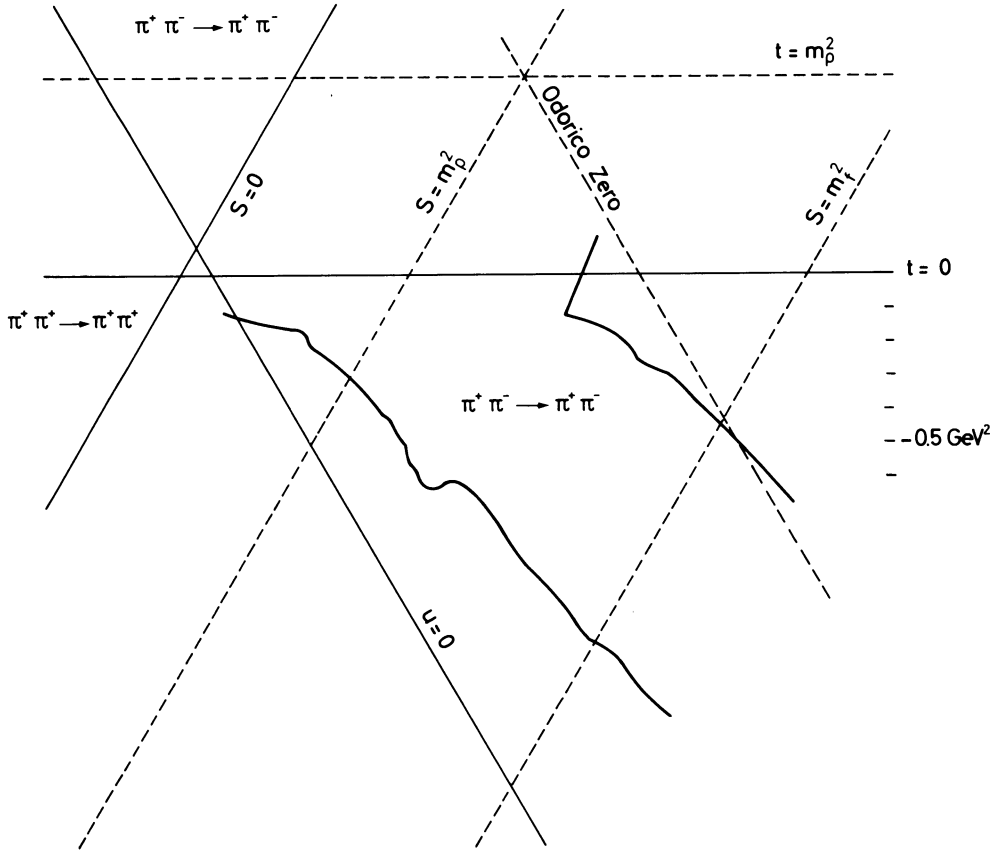

Figure 17 The zero contours in the Mandelstam plot

associated[33] with the on-shell appearance of the Adler zero. The contour z_2 is reasonably consistent with the proposal by Odorico[8] that the double-pole killing zeros propagate along straight lines.

c) $\pi\pi$ partial waves :

To determine the $\pi\pi$ partial waves in the inelastic region it remains to specify the over-all phase at each $M_{\pi\pi}$. The possible values are limited by the unitarity constraints on the three partial waves. Moreover each partial wave must be reasonably continuous as a function of $M_{\pi\pi}$. Indeed, the presence of the f resonance in this mass region essentially removes the phase ambiguity. Suitably rotating the two solutions of Fig. 14 we obtain the partial waves shown in Figs. 18 and 19 together with their unitarity circles. Solution 1 is selected as the physical solution for the following reasons. In the region just above the $K\bar{K}$ threshold the $I=0$ S wave of solution 2 contributes very little to $\sigma(\pi\pi \to K\bar{K})$ contrary to the data. Further, the M matrix fits across the $K\bar{K}$ threshold prefer to join solution 1 to the physical solution below threshold. Finally, for $M_{\pi\pi} > 1.26$ GeV the magnitude of the S wave of solution 2 violates unitarity.

Notice that in Fig. 18 the P wave lies outside its unitarity circle for $M_{\pi\pi} \geq 1.26$ GeV. The reason we believe that the picture is basically correct as it stands, apart from this violation, is the neglect of the $\pi\pi$ F wave. The data that we used did not include the $J=5$ or higher moments and so we were unable to determine the $L=3$ partial wave. On the other hand we investigated the stability of the analysis to the inclusion of elastic F waves with $\delta_F \lesssim 5^\circ$. We find that the D wave is essentially unchanged and that the S wave is only slightly altered. The major change is in the P wave which decreases and rotates in the clockwise direction (for example, for $\delta_F = 4^\circ$ at $M_{\pi\pi} = 1.38$ GeV, we find $\Delta\delta_P = -10^\circ$ and $\Delta r_P / r_P = -0.12$).

To determine the parameters of the f resonance we fit the resonance form, Eq. (17) with

$$D_2(y) = 9 + 3y + y^2,$$

to the values of $|r_D|$ in the region $1.14 < M_{\pi\pi} < 1.38$ GeV. Since $|r_D|$ is well determined and independent of the over-all phase this procedure should be reliable. We find

$$M_f = 1271 \pm 2 \text{ MeV}, \qquad \Gamma_f = 182 \pm 4 \text{ MeV}$$

$$x_f = 0.81 \pm 0.01, \qquad y_f = 0.70 \pm 0.08 f.$$

$\pi\pi$ PARTIAL WAVES ($1.0 < M_{\pi\pi} < 1.4$ GeV)

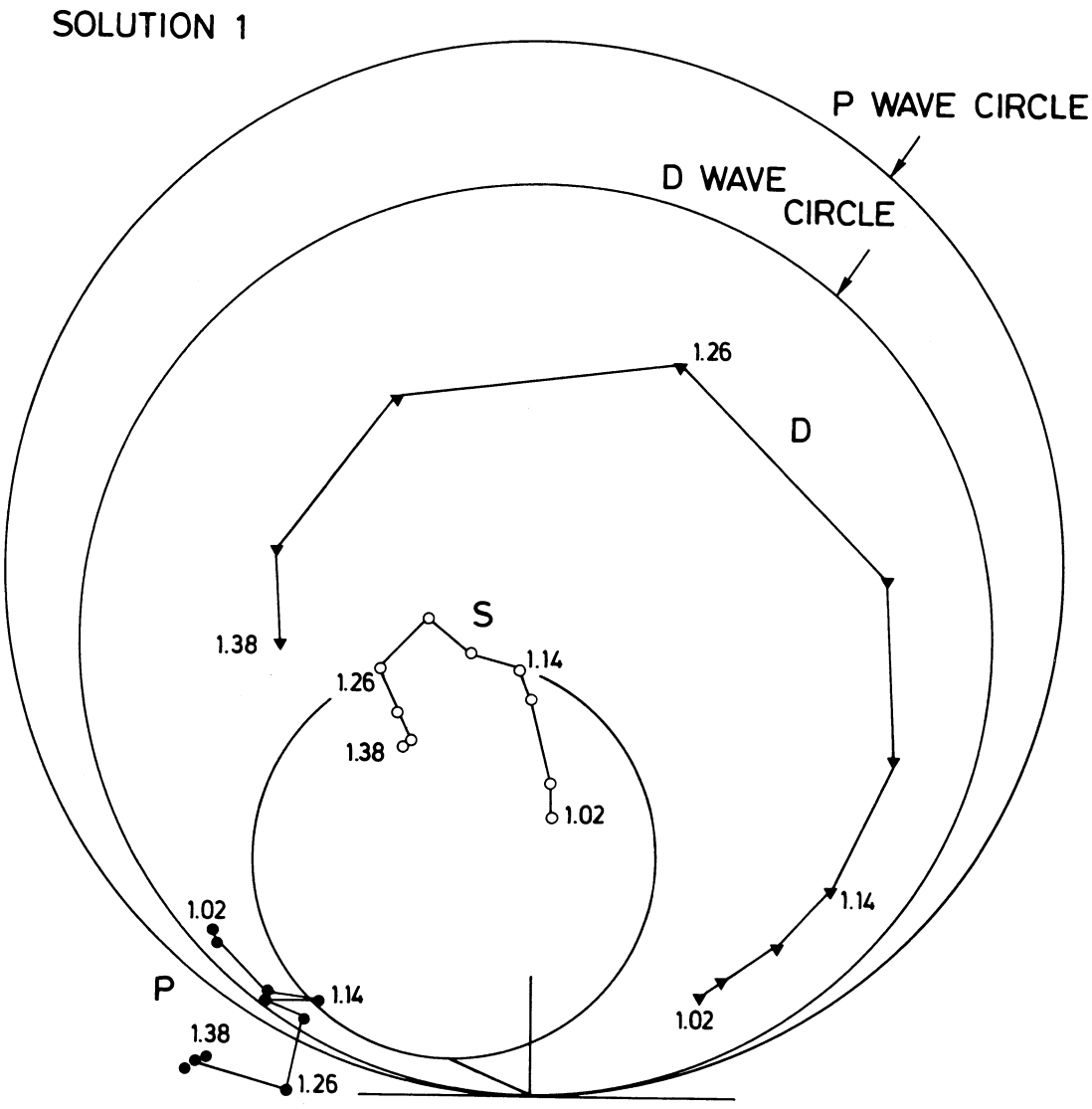

Figure 18 The physical solution, solution 1, for the $\pi\pi$ partial wave amplitudes above 1 GeV. The I = 0 S wave, P wave and I = 0 D wave unitarity circles are in the ratio $\frac{2}{3} : \sqrt{3} : \frac{2}{3}\sqrt{5}$.

$\pi\pi$ PARTIAL WAVES ($1.0 < M_{\pi\pi} < 1.4$ GeV)

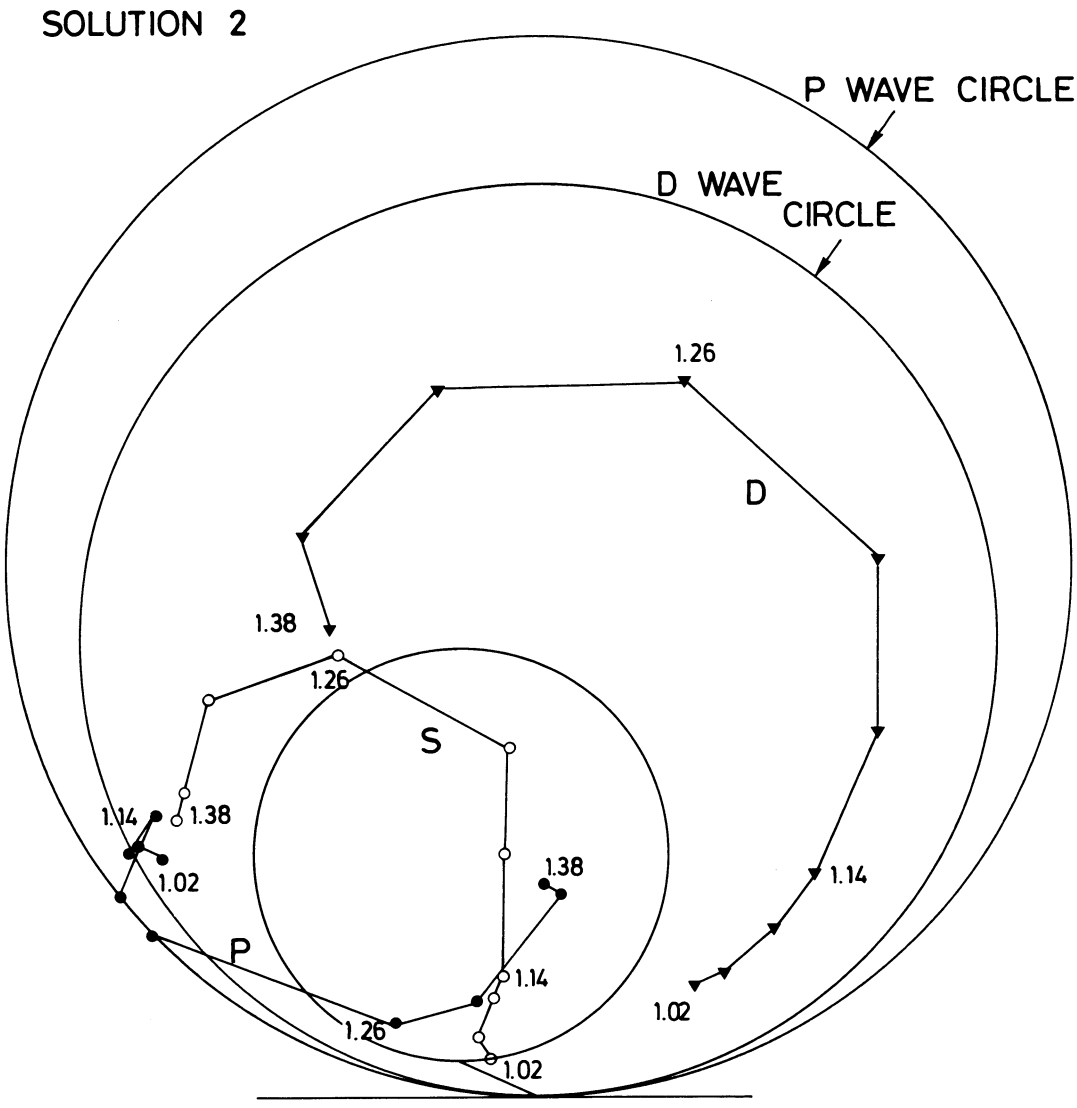

Figure 19 The $\pi\pi$ partial waves for the unphysical solution, solution 2.

Figure 18 also indicates the presence of a resonant $I = 0$ S wave under the f, with a mass and width of roughly 1240 and 200 MeV respectively. To confirm these parameters we wish to include F waves and to extend the analysis to higher $M_{\pi\pi}$.

d) Phase coherent analysis :

As in the elastic region we have performed a phase shift analysis with a simplified form of parametrization, cf. Eqs. (20). We neglect A_2 exchange and assume that the absorptive background C is real relative to π exchange. We include a common slope factor, $\exp\left[b(t - \mu^2)\right]$, in all amplitudes. In addition to the parameters C and b, we have the magnitudes and relative phases of the S, P, D partial waves. In each 40 MeV mass bin these seven parameters give a good fit to the s channel moments in the region $0 < -t < 0.1$ GeV^2. The results for C, b and the $I = 0$ S wave are shown in Fig. 11, where the over-all phase has been fixed by requiring the P wave to be elastic. The partial waves are very similar to the solution 1 results of Fig. 18. Moreover, we also find a solution almost identical to solution 2.

A surprising result[34,35] is the rapid decrease of the strength of absorption, C, with increasing $M_{\pi\pi}$. This could be anticipated from the data by inspection of the positions of the cross-over zeros in the s channel $< Y_1^J >$ moments. For example, comparing the moments shown at $M_{\pi\pi} = 710$ MeV (Fig. 6) and at $M_{\pi\pi} = 1140$ MeV (Fig. 13) we see that at the higher mass the zeros occur at smaller $|t|$. The Williams' model, with $C = 1$, is known[36,15] to give a good description of the small t data in the ρ region, but is unsatisfactory in the f region.

8. $K\bar{K}$ THRESHOLD

The data and the phase shift results indicate a dramatic effect in the $I = 0$ S wave in the region of the $K\bar{K}$ threshold. Moreover, the effect occurs in a small range of $M_{\pi\pi}$. Up to 980 MeV and beyond 1 GeV the partial wave amplitudes do not change rapidly, and yet, in between, the $I = 0$ S wave amplitude has altered drastically. Clearly to investigate this effect properly we require the moments for $\pi^- p \to \pi^- \pi^+ n$, together with those for $\pi^- p \to K^- K^+ n$ (and $K_1^0 K_1^0 n$), in smaller $M_{\pi\pi}$ bins. However, even a study of the existing data and phase shifts is illuminating.

First we performed an S, P, D wave M matrix fit directly on the $\pi^- p \to \pi^- \pi^+ n$ data in the region $920 < M_{\pi\pi} < 1080$ MeV. That is we parametrized the production amplitudes as a function of $M_{\pi\pi}$, as well as of t. We did fits with and without effective range terms in the M matrix. As an alternative approach we also fitted the $I = 0$ S wave phase shifts (of Figs. 7, 18, 19) to an M matrix over the same $M_{\pi\pi}$ region. We discuss the

results of the second method first. The preferred fit was the one which joined the phase shifts of solution 1 below the $K\bar{K}$ threshold to those of solution 1 above threshold. An example of such a fit is shown in Fig. 20, corresponding to an $I = 0$ two channel $(\pi\pi, K\bar{K})$ M matrix

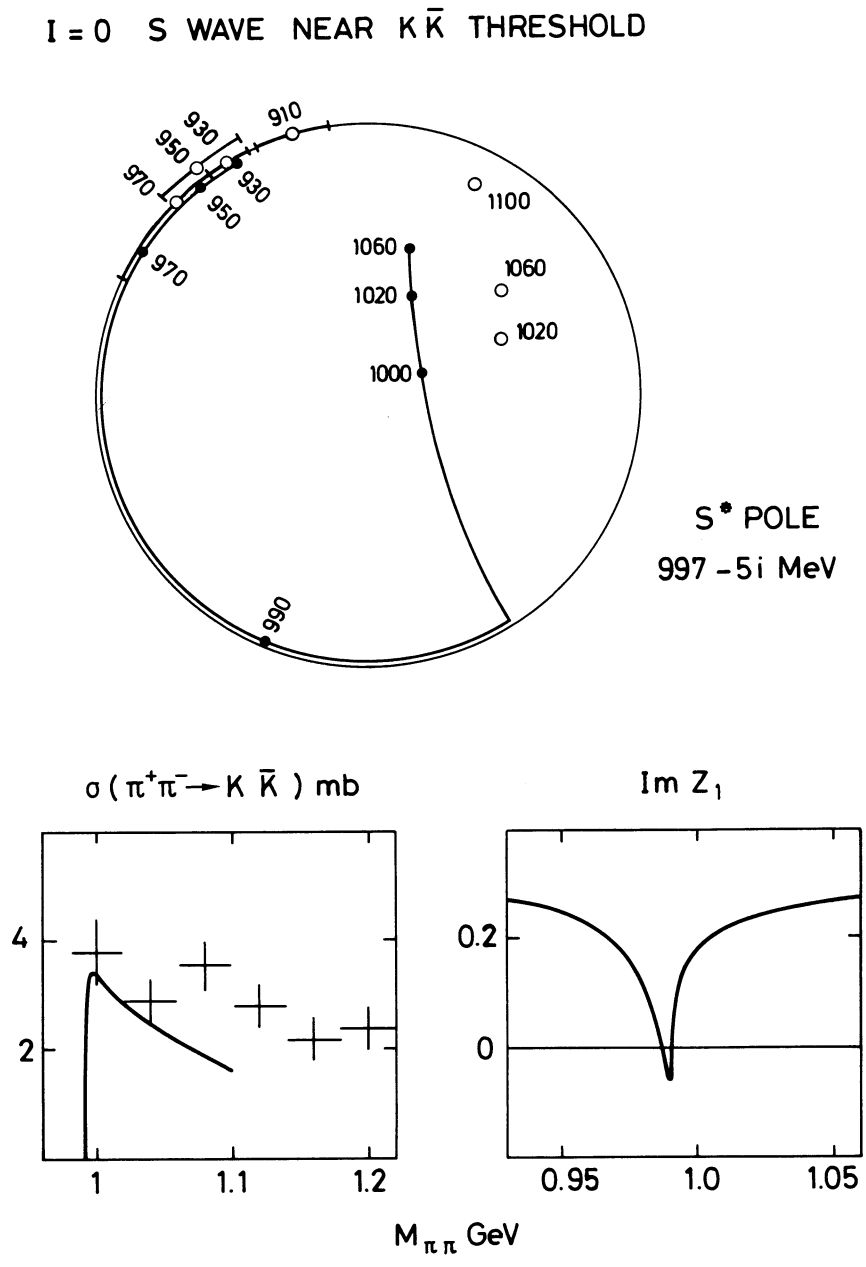

Figure 20 The $I = 0$ S wave unitarity circle. The open circles are solution 1 of the energy independent analysis. The black dots come from the sample M matrix fit. The last curve is the behaviour of Im z_1 (cf. Fig. 16) calculated using the M matrix and assuming that $\delta^2_S = -20^\circ$, $\delta_P = 156^\circ$, $\delta^0_D = 6^\circ$.

$$M = \begin{pmatrix} 0.27 & 0.83 \\ 0.83 & -0.09 \end{pmatrix} f^{-1} \qquad (25)$$

The resulting S wave amplitude has a pole on the second Riemann sheet of the complex energy plane at

$$S^*(\text{pole}) = 997 - i5 \text{ MeV.} \qquad (26)$$

The existence of such a pole was suggested by Hoang[37] and subsequently confirmed by Protopopescu et al.[24] whose favoured solution gives $S^* = 997 - i27$ MeV. In Fig. 20 we compare the S wave contribution to $\sigma(\pi^+\pi^- \to K\bar{K})$, calculated from Eq. (25) to the data of Ref. 24. The narrower the peak in this cross-section, the larger the S^* coupling to the $K\bar{K}$ channel[9].

It is interesting to compare the above results with our first M matrix fit directly to the $\pi^-\pi^+n$ data. There we find a wider S^* structure. The reason is that, although the fit basically follows phase shift solution 1, it jumps to solution 2 for a range of $M_{\pi\pi}$ in the immediate vicinity of the $K\bar{K}$ threshold. This is likely to happen in any energy dependent fit to such a narrow structure, and is well illustrated in Fig. 7 where the solution of Protopopescu et al.[24] goes from the region of our solution 1 to solution 2 just below the $K\bar{K}$ threshold. The situation is more confused as the energy independent analysis of Ref. 5 showed some indication of preferring a switch from solution 1 to solution 2 just below the $K\bar{K}$ threshold.

The rapidly changing S partial wave in the region of the $K\bar{K}$ threshold produces a sharp structure in the zero contours. For example, in Fig. 20 we show the behaviour of Im z_1 calculated using the parameters of Eq. (25) and reasonable constant values for the other phase shifts. In the energy dependent fit Im z_1 is found to dip to zero less sharply. Comparison with the energy independent results of Fig. 16 again emphasizes the need for data in smaller $M_{\pi\pi}$ bins in this mass region.

Since we estimate such a small width for the S^* it is clear that the parameters of Eqs. (25) and (26) are not reliably determined from the data in 20-40 MeV mass bins. However, the point we wish to make is that the S^* structure appears to be narrower than hitherto thought.

ACKNOWLEDGEMENTS

We thank C. Michael, D. Morgan and W. Ochs for interesting discussions.

REFERENCES

1. C. Goebel, Phys.Rev.Letters 1, 337 (1958).
2. G.F. Chew and F.E. Low, Phys.Rev.Letters 113, 1640 (1959).
3. See, for example, the review articles by :
   P.E. Schlein, Proc. of the International School of Subnuclear Physics, Erice (1970) ;
   J.L. Petersen, Physics Reports 2C, 157 (1971) ;
   D. Morgan, Proc. of the VII Finnish Summer School, Loma-Koli (1972).
4. CERN-Munich Collaboration : G. Grayer, B. Hyams, C. Jones, P. Schlein, P. Weilhammer, W. Blum, H. Dietl, W. Koch, E. Lorenz, G. Lütjens, W. Männer, J. Meissburger, W. Ochs and U. Stierlin, to be published.
5. G. Grayer et al., Experimental Meson Spectroscopy (AIP), Proc. of III Philadelphia Conference (1972), p. 5.
6. G. Grayer et al., Phys.Letters 35B, 610 (1971).
7. J.T. Carroll et al., Phys.Rev.Letters 28, 318 (1972).
8. R. Odorico, Phys.Letters 38B, 411 (1972).
9. S.M. Flatté et al., Phys.Letters 38B, 232 (1972).
10. G.L. Kane and M. Ross, Phys.Rev. 177, 2353 (1969) ;
    C.D. Froggatt and D. Morgan, Phys.Rev. 187, 2044 (1969).
11. G.L. Kane, Experimental Meson Spectroscopy (Columbia University Press, 1970), p. 1.
12. A. Kotanski and K. Zalewski, Nuclear Phys. B4, 559 (1968) ; B20, 236 (1970) E ; B22, 317 (1970).
13. G. Grayer et al., Nuclear Phys. B50, 29 (1972).
14. W. Männer, Contribution to International Conference on $\pi\pi$ Scattering and Associated Topics, Tallahassee (March 1973).
15. P. Estabrooks and A.D. Martin, Phys.Letters 41B, 350 (1972).
16. See, for example :
    M. Ross, F.S. Henyey and G.L. Kane, Nuclear Phys. B23, 269 (1970).
17. C. Michael, Springer Tracts of Modern Physics 55, 174 (1970).
18. P.K. Williams, Phys.Rev. D1, 1312 (1970).
19. C.D. Froggatt and D. Morgan, Phys.Letters 40B, 655 (1972).
20. J.D. Kimel and E. Reya, Phys.Letters 42B, 249 (1972).
21. W. Hoogland, Contribution to International Conference on $\pi\pi$ Scattering and Associated Topics, Tallahassee (March 1973).
22. P. Baillon et al., Phys.Letters 38B, 555 (1972).
23. J.P. Baton, G. Laurens and J. Reignier, Phys.Letters 33B, 525 and 528 (1970).
24. S.D. Protopopescu et al., Phys.Rev. D7, 1279 (1973).
25. See, for example :
    G.C. Fox, Experimental Meson Spectroscopy (AIP), Proc. of III Philadelphia Conference (1972).
26. W.D. Apel et al., Phys.Letters 41B, 542 (1972).
27. E.I. Shibata, D.H. Frisch and M.A. Wahlig, Phys.Rev.Letters 25, 1227 (1970) ;
    A. Skuja et al., LBL Preprint 1020 (March 1973).
28. A. Barbaro-Galtieri, Advances in Particle Physics (Wiley, 1968), Vol. 2, p. 212.

29. W. Beusch, Experimental Meson Spectroscopy (Columbia University Press, 1970), p. 185.
30. A. Gersten, Nuclear Phys. B12, 537 (1969).
31. E. Barrelet, Nuovo Cimento 8A, 331 (1972).
32. C. Schmid, Proc. of 1971 Amsterdam International Conference on Elementary Particles (North Holland, 1972), p. 275.
33. M. Pennington and C. Schmid, LBL Preprint 1005 (1972).
34. W. Ochs and F. Wagner, to be published in Nuclear Phys.
35. A.D. Martin and P. Estabrooks, to be published in Proc. of VIII Rencontre de Moriond (1973).
36. P. Baillon et al., Phys.Letters 35B, 453 (1971).
37. F.T. Hoang, Nuovo Cimento 61A, 325 (1969).